

# Black Hole Spin via Continuum Fitting and the Role of Spin in Powering Transient Jets

Jeffrey E. McClintock · Ramesh Narayan ·  
James F. Steiner

Received: 2013 March 3 / Accepted: 2013 June 24

**Abstract** The spins of ten stellar black holes have been measured using the continuum-fitting method. These black holes are located in two distinct classes of X-ray binary systems, one that is persistently X-ray bright and another that is transient. Both the persistent and transient black holes remain for long periods in a state where their spectra are dominated by a thermal accretion disk component. The spin of a black hole of known mass and distance can be measured by fitting this thermal continuum spectrum to the thin-disk model of Novikov and Thorne; the key fit parameter is the radius of the inner edge of the black hole’s accretion disk. Strong observational and theoretical evidence links the inner-disk radius to the radius of the innermost stable circular orbit, which is trivially related to the dimensionless spin parameter  $a_*$  of the black hole ( $|a_*| < 1$ ). The ten spins that have so far been measured by this continuum-fitting method range widely from  $a_* \approx 0$  to  $a_* > 0.95$ . The robustness of the method is demonstrated by the dozens or hundreds of independent and consistent measurements of spin that have been obtained for several black holes, and through careful consideration of many sources of systematic error. Among the results discussed is a dichotomy between the transient and persistent black holes; the latter have higher spins and larger masses. Also discussed is recently discovered evidence in the transient sources for a correlation between the power of ballistic jets and black hole spin.

**Keywords** black hole physics · accretion disks · X-ray binaries · stars: winds, outflows

## 1 Introduction

In his Ryerson Lecture, Chandrasekhar (1975) described the Kerr solution as the “most shattering experience” of his entire scientific life. He found himself “shuddering before the beautiful, the incredible fact” that each of the many trillions of black holes in the universe is completely described by a single pair of numbers that specify the

---

J. E. McClintock, R. Narayan, and J. F. Steiner  
Harvard-Smithsonian Center for Astrophysics, 60 Garden Street, Cambridge, MA 02138 USA  
email: jem@cfa.harvard.edu; narayan@cfa.harvard.edu; jsteiner@cfa.harvard.edu

black hole’s mass and its spin <sup>1</sup>. In Chandrasekhar’s time, 1910–1995, the masses of Cyg X-1 and three other stellar black holes had been estimated (Webster & Murdin 1972; Bolton 1972; Cowley et al. 1983; McClintock & Remillard 1986; Remillard et al. 1992; Shahbaz et al. 1994). Today, accurate dynamical mass measurements have been achieved for more than a dozen stellar black holes (McClintock & Remillard 2006; Özel et al. 2010; Orosz et al. 2011a; Steeghs et al. 2013), as well as for several supermassive black holes, e.g., Sgr A\* (Ghez et al. 2008; Gillessen et al. 2009), NGC 4258 (Herrnstein et al. 2005), and others (Gültekin et al. 2009, and references therein).

In 1989, the first practical approach to measuring black hole spin was suggested by Fabian et al. (1989), namely, modeling the relativistically-broadened Fe K emission line emitted from the inner accretion disk. The first compelling observation of such a line was reported just two months before Chandrasekhar died (Tanaka et al. 1995). Presently, the spins of more than a dozen black holes have been estimated by modeling the “reflected” spectrum of an accretion disk, which includes as its most prominent feature the Fe K line. For a review of this method of measuring black hole spin, we refer the reader to Reynolds (2013).

It was not until 1997 that a new approach to measuring black hole spin – the continuum-fitting method – which is the subject of this chapter, was pioneered by Zhang et al. (1997). In brief, in applying this method one fits the thermal continuum spectrum of a black hole’s accretion disk to the relativistic thin-disk model of Novikov & Thorne (1973) and thereby determines the radius of the inner edge of the disk. One then identifies this radius with the radius of the innermost stable circular orbit ( $R_{\text{ISCO}}$ ), which is simply related to the spin parameter  $a_*$  (Bardeen et al. 1972). The method is simple: It is strictly analogous to measuring the radius of a star whose flux, temperature and distance are known. By this analogy, it is clear that it is essential to know the luminosity of the accretion disk; hence, one must have estimates of the source distance  $D$  as well as the disk inclination  $i$ . Additionally, one must know  $M$  in order to scale  $R_{\text{ISCO}}$  and thereby determine  $a_*$ .

In 2006, the continuum-fitting method was employed to estimate the spins of three stellar black holes (Shafee et al. 2006; McClintock et al. 2006). Presently, ten spins have been measured using this method (Section 6). Not only is the continuum-fitting method simple, it is also demonstrably robust. For example, there is strong observational and theoretical evidence (discussed in Section 4) that the disk is truncated quite sharply at  $R_{\text{ISCO}}$ . Furthermore, there is an abundance of suitable X-ray spectral data for many black holes; consequently, for a given black hole one can typically obtain tens or even hundreds of independent measurements of spin that agree to within a few percent (Section 4.1). The one open question for this method is whether the black hole’s spin is aligned with the orbital angular momentum vector of the inner disk (Section 5.4). Meanwhile, a limitation of the continuum-fitting method is that it is only readily applicable to stellar black holes (but see Jolley et al. 2009; Czerny et al. 2011), while the Fe K method is applicable to both stellar and supermassive black holes (Reynolds 2013).

In order to obtain secure measurements of spin using the continuum-fitting method, and to establish the reliability of this method, substantial and comparable effort is required on three fronts: (1) The selection and fitting of X-ray spectral data to the Novikov-Thorne model (in conjunction with ancillary models); (2) testing and explor-

---

<sup>1</sup> Spin is commonly expressed in terms of the dimensionless parameter  $a_* \equiv cJ/GM^2$ , where  $J$  and  $M$  are respectively the angular momentum and mass of the black hole.

ing extensions of the Novikov-Thorne model via general relativistic magnetohydrodynamic (GRMHD) simulations; and (3) obtaining accurate estimates of  $D$ ,  $i$  and  $M$ . The first two topics are discussed in Sections 3–5. Concerning the third topic, we refer the reader to recent papers on the measurements of these crucial parameters for M33 X-7 (Orosz et al. 2007); LMC X-1 (Orosz et al. 2009); A0620–00 (Cantrell et al. 2010); XTE J1550–564 (Orosz et al. 2011b); Cyg X-1 (Reid et al. 2011; Orosz et al. 2011a); H1743–322 (Steiner et al. 2012a); and GRS 1915+105 (Steehgs et al. 2013). The uncertainties in  $D$ ,  $i$  and  $M$  are critically important because they dominate the error budget in the final determination of  $a_*$ , including the error incurred by reliance on the Novikov-Thorne disk model (Section 5).

Initial efforts are under way to use the available continuum-fitting spin data to investigate the formation and evolution of black holes, as well as their host systems (e.g., Lee et al. 2002; Wong et al. 2012), and to understand how a black hole interacts with its environment (e.g., Wang et al. 2003; Cooke et al. 2008). The most important application to date of spin data is the discovery of a long-predicted correlation between jet power and black hole spin, which is the subject of Section 7. Very recently, Russell et al. (2013) challenged the validity of this correlation; Section 7.4 answers this challenge.

## 2 Stellar Black Holes in X-ray Binaries

There are 24 confirmed black hole binaries: the 23 listed in Table 1 in Özel et al. (2010) plus H1743–322 (Steiner et al. 2012a)<sup>2</sup>. A schematic sketch to scale of 21 of these confirmed black-hole systems is shown in Figure 1.

For decades, it has been customary to define two classes of X-ray binaries, commonly referred to as LMXBs (low-mass X-ray binaries) and HMXBs (high-mass X-ray binaries), based on whether the mass of the secondary star is relatively low or relatively high (e.g., Bradt & McClintock 1983). Here, we use a different classification scheme that differentiates two distinct classes of black hole binaries by the primary mode of mass transfer to the black hole and the effect that this has on the stability of the X-ray source (White et al. 1995).

The black holes in five of the 24 systems are steadily fed by the winds of massive O-supergiant or Wolf-Rayet companions, and consequently their bolometric X-ray luminosities are relatively stable. Sketches of three of these systems (M33 X-7, LMC X-1 and Cyg X-1) appear in the top-right corner of Figure 1. We refer to these systems and their black holes as “persistent.”

The black holes in the remaining systems are fed by Roche lobe overflow through the L1 point, and all of them have been observed to vary in luminosity by factors of  $> 100$  ( $\sim 10^8$  in several extreme cases; e.g., see Narayan & McClintock 2008). We refer to these systems and their black holes as “transient.”

---

<sup>2</sup> Apart from H1743–322, our selection is based on firm dynamical evidence, and we therefore exclude some important systems for which there is significant evidence that the primary is a black hole, e.g., Cyg X-3 (Zdziarski et al. 2013), or a strong presumption that it is, e.g., SS433 (Begelman et al. 2006) and 4U 1957+11 (Nowak et al. 2012)

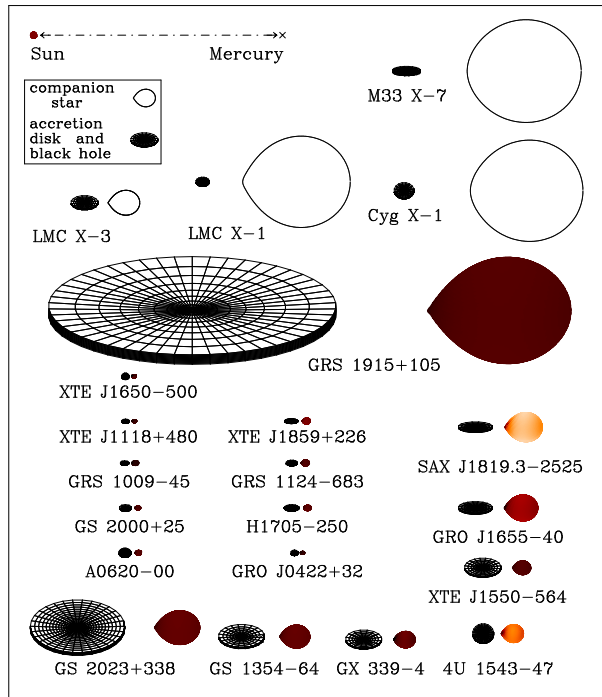


**Fig. 1** Schematic sketch to scale of 21 black hole binaries (see scale and legend in the upper-left corner). The tidally-distorted shapes of the companion stars are accurately rendered in Roche geometry. The black holes are located in the center of the disks. A disk’s tilt indicates the inclination angle  $i$  of the binary, where  $i = 0$  corresponds to a system that is viewed face-on; e.g.,  $i = 21^\circ$  for 4U 1543-47 (bottom right) and  $i = 75^\circ$  for M33 X-7 (top right). The size of a system is largely set by the orbital period, which ranges from 33.9 days for the giant system GRS 1915+105 to 0.2 days for tiny XTE J1118+480. Three well-studied persistent systems (M33 X-7, LMC X-1 and Cyg X-1) are located in the upper-right corner. The other 18 systems are transients. (Figure courtesy of J. Orosz.)

## 2.1 Persistent Black Hole Binaries

These systems are distinguished by the large masses of their secondary stars ( $20 M_\odot - 70 M_\odot$ ) and by the extreme optical/UV luminosities of these stars, which exceed the X-ray luminosities of their black hole companions. Consequently, the effects of X-ray heating are minimal and the optical star dominates the optical properties of the system. The key distinguishing feature of these systems is their X-ray persistence, which is a consequence of the star’s massive stellar wind ( $\sim 10^{-5} - 10^{-8} M_\odot \text{ yr}^{-1}$ ), a significant fraction of which is captured by the black hole.

Because the secondaries are massive these systems are obviously young ( $\lesssim 10^7 \text{ yr}$ ). They are also very rare: There is only one confirmed system in the Galaxy, Cyg X-1, and, despite many deep *Chandra* and *XMM-Newton* X-ray observations of Local Group galaxies, only four other such systems have been discovered, one each in the LMC, M33, IC 10 and NGC 300.

In this review, we do not consider further the two persistent systems that contain Wolf-Rayet secondaries, namely IC 10 X-1 and NGC 300 X-1, because the masses of their black holes depend strongly on the very uncertain masses of their secondaries, and also because no attempt has so far been made to estimate their spins. By contrast, the three remaining persistent systems – M33 X-7, LMC X-1 and Cyg X-1 – have well-determined values of both mass and spin (see Section 6). Relative to the black hole primaries in the transient systems (apart from GRS 1915+105), the black holes in these three persistent systems have large masses,  $M = 11 - 16 M_\odot$ , and high spins that range from  $a_* = 0.84$  to  $a_* > 0.95$ , a point that we return to in Section 6.1.

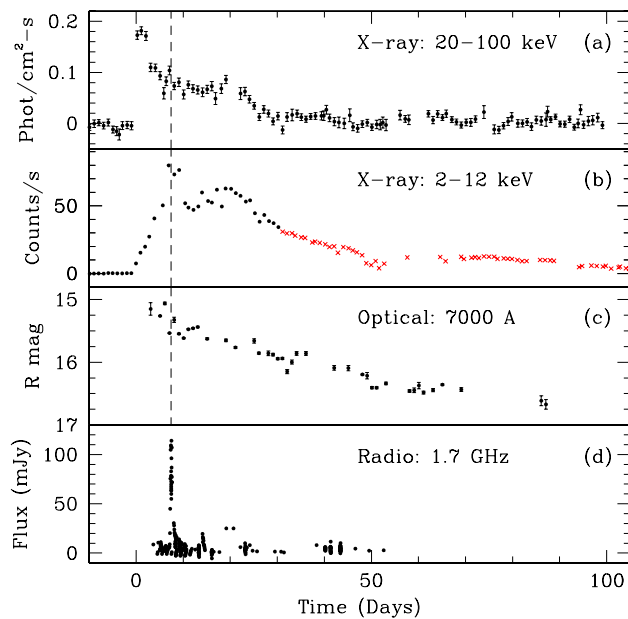


**Fig. 2** Outburst cycle of XTE J1859+226 in 1999. The dashed line (top three panels) marks the time of peak radio flux (panel d). The  $\approx 1$ -day radio spike (panel d) is shown fully resolved in Figure 2 in Brocksopp et al. (2002). The red crosses (panel b) indicate times when the X-ray spectrum is dominated by the thermal component. These *BATSE* and *RXTE/ASM* X-ray, and Merlin (and other) radio data (panels a, b and d, respectively) appear in Figure 1 in Brocksopp et al. (2002) and the optical data (panel c) appear in Figure 2 in Sánchez-Fernández et al. (2001). For further details, consult the references.

## 2.2 Transient Black Hole Binaries

With few exceptions, the 18 transient black hole binaries (hereafter simply referred to as transients) manifest and then rise to maximum X-ray luminosity on a timescale of several days, thereafter returning to a quiescent state over a period of many tens or hundreds of days, as illustrated in Figure 2. The masses of the black holes in these systems are relatively low, as are their spins (with the exception of GRS 1915+105), and their orbital periods range widely from 0.2–33.9 days. By comparison, the orbital periods of the persistent systems span a relatively narrow range. The transients are, on average, likely Gyrs old (White & Ghosh 1998; Fragos et al. 2013).

During a major outburst, the peak luminosities of transient sources approach the Eddington limit (Steiner et al. 2013), while in quiescence their luminosities are typically in the range  $10^{-8.5}$  to  $10^{-6}$  of Eddington (Narayan & McClintock 2008). Figure 2 shows X-ray, optical and radio light curves of a typical short-period transient. The optical emission is generated largely by reprocessing of X-rays in the accretion disk, and the radio outburst is primarily the result of synchrotron emission produced in a jet. The ballistic jets, which are the subject of Section 7, are launched very near the time of peak radio emission (panel d), which in the case of XTE J1859+226 occurred just 0.5 days after the X-ray luminosity (panel b) peaked. Spin can be reliably measured when the thermal component dominates the spectrum during the latter part of the outburst cycle (panel b). For a complete and state-coded version of the X-ray light curve of XTE J1859+226, see Figure 8b in Remillard & McClintock (2006).

There are several oddballs among the transient systems: Four have relatively massive secondaries,  $\sim 2-6 M_{\odot}$ , compared to the typical value of  $\lesssim 1 M_{\odot}$  (Charles & Coe 2006). GRS 1915+105 has remained very luminous continuously since its appearance

in 1992, and GX 339-4 never reaches a deep quiescent state (McClintock & Remillard 2006). LMC X-3 is almost always active and highly variable (Section 4.1), although it does have extended low states (Smale & Boyd 2012).

### 3 The Continuum-Fitting Method

The two foundations of the continuum-fitting method are (1) the existence of an ISCO for a test particle orbiting a black hole and (2) the strong observational and theoretical evidence that – for a wide range of conditions – accretion disks in black hole binaries are truncated quite sharply at the ISCO radius. In this section, we first discuss the physics of these disks, and we close by describing the mechanics of continuum fitting.

#### 3.1 Accretion Disk Theory

The basic physics of black hole accretion is straightforward (Frank et al. 2002; Kato et al. 2008; Abramowicz & Fragile 2013). Gas with angular momentum flows in from the outside and settles into a circular orbit stabilized by centrifugal force. The gas steadily loses angular momentum as a result of magnetic stresses from the magnetorotational instability (Balbus & Hawley 1998), whose effect is often approximated via the  $\alpha$ -viscosity prescription of Shakura & Sunyaev (1973). As the gas loses angular momentum, it moves inward, occupying at each instant a circular orbit appropriate to its instantaneous angular momentum. The inward drift continues until the gas reaches the radius of the ISCO,  $R_{\text{ISCO}}$ . Inside  $R_{\text{ISCO}}$ , no stable circular orbits are available and the gas falls dynamically into the black hole.

As described above, the ISCO represents a major transition point in disk physics, where gas switches from slow viscous accretion on the outside to inviscid free-fall on the inside. The ISCO is thus effectively the inner edge of the disk. Correspondingly, information on the linear dimensions of the radius  $R_{\text{ISCO}}$  is imprinted on the emitted radiation. Since  $R_{\text{ISCO}}$  varies monotonically with the black hole spin parameter  $a_*$  (Bardeen et al. 1972), as illustrated in Figure 3a, it is thus possible to measure  $a_*$  by modeling the disk emission.

The model of choice for this purpose is that described by Novikov & Thorne (1973), hereafter referred to as the NT model, which is the relativistic generalization of the thin accretion disk model of Shakura & Sunyaev (1973). Using nothing more than the Kerr metric, basic conservation laws of mass, momentum, angular momentum and energy, and assumptions of axisymmetry and steady state, the NT model (see also Page & Thorne 1974; Riffert & Herold 1995) derives an analytical formula for the differential luminosity  $dL(R)/dR$  emitted by the disk as a function of radius  $R$ .

The solid lines in Figure 3b show for three values of  $a_*$  the differential disk luminosity predicted by the NT model. The disk flux vanishes at  $R_{\text{ISCO}}$  because the model has, by assumption, no viscous stress inside this radius (see Section 4.2 for further discussion). More importantly, the peak emission occurs at a radius that tracks the ISCO (it is a factor of  $\sim 2 - 3$  larger than  $R_{\text{ISCO}}$ ). This means that the radiation is emitted from a progressively smaller effective area, roughly  $\propto R_{\text{ISCO}}^2$ , as the black hole spin increases. Therefore, for a given total disk luminosity, the temperature of the emitted radiation increases with increasing  $a_*$ . This is the key physical effect that underlies the

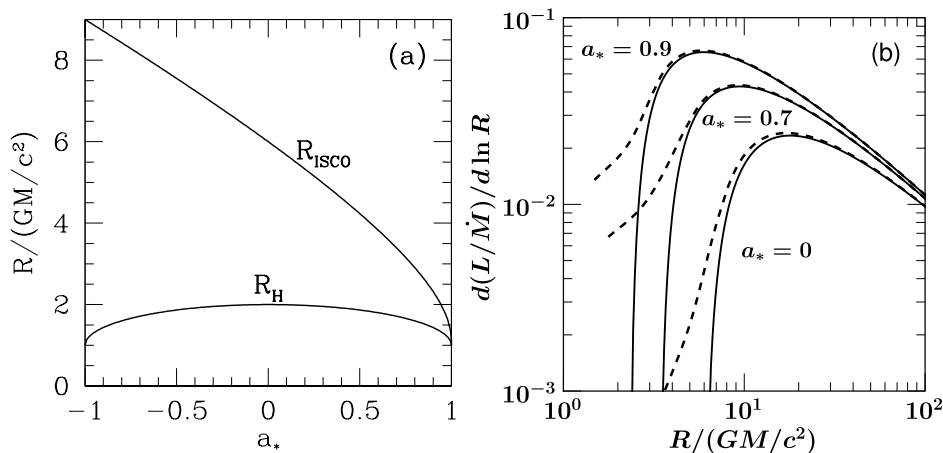


**Fig. 3** (a) Radius of the ISCO  $R_{\text{ISCO}}$  and of the horizon  $R_{\text{H}}$  in units of  $GM/c^2$  plotted as a function of the black hole spin parameter  $a_*$ . Negative values of  $a_*$  correspond to retrograde orbits. Note that  $R_{\text{ISCO}}$  decreases monotonically from  $9GM/c^2$  for a retrograde orbit around a maximally spinning black hole, to  $6GM/c^2$  for a non-spinning black hole, to  $GM/c^2$  for a prograde orbit around a maximally spinning black hole. (b) Profiles of  $d(L/\dot{M})/d \ln R$ , the differential disk luminosity per logarithmic radius interval normalized by the mass accretion rate, versus radius  $R/(GM/c^2)$  for three values of  $a_*$ . Solid lines are the predictions of the NT model. The dashed curves from Zhu et al. (2012), which show minor departures from the NT model, are discussed in Section 5.2.

continuum-fitting method. By measuring the characteristic temperature and luminosity of the disk emission, and applying the NT model, one is able to estimate both  $a_*$  and the mass accretion rate  $\dot{M}$ .

As should be clear from the above, the accuracy of the continuum-fitting method ultimately depends on the reliability of the NT model; this issue is discussed further in Sections 4.2 and 5.2. It also depends on our ability to calculate the spectrum of the radiation, which would be trivial if the disk radiated as a perfect blackbody. Unfortunately, because electron scattering plays a prominent role at the X-ray temperatures found in black hole binaries, the emitted spectrum is substantially harder than a blackbody spectrum of the same flux. Hence it is necessary to employ detailed disk atmosphere models. Most of the work to date is based on the atmosphere model BHSPEC developed by Davis & Hubeny (2006), which is discussed in Sections 3.2 and 5.3.

### 3.2 Continuum Fitting in Practice

In broad outline, one fits the X-ray continuum spectrum to the Novikov-Thorne model of a thin accretion disk with other spectral components as needed, principally a Compton component. As stressed in Sections 1 and 5, in order to obtain useful constraints on  $a_*$ , one must inform the fitting process by inputting accurate values of the external parameters  $D$ ,  $i$  and  $M$ . The spectral fit returns two output parameters: the spin  $a_*$  and the mass accretion rate  $\dot{M}$ . An important derived quantity is the Eddington-scaled luminosity of the disk component  $L(a_*, \dot{M})/L_{\text{Edd}}$ .

In practice, one usually fits the thermal component using KERRBB2 (McClintock et al. 2006)<sup>3</sup>, which is a hybrid code implemented in XSPEC (Arnaud 1996) that combines the capabilities of two relativistic disk models, BHSPEC (Davis et al. 2005) and KERRBB (Li et al. 2005). This latter model, KERRBB, which is a straightforward implementation of the analytic Novikov-Thorne model, has three principal fit parameters:  $a_*$ ,  $M$ , and the spectral hardening factor  $f$ , which relates the observed color temperature to the effective temperature,  $f = T/T_{\text{eff}}$ .

In fitting the disk component with KERRBB, it is quite generally the case that one can only determine two parameters, a shape parameter (e.g.,  $a_*$  or  $T$ ) and a normalization constant (e.g.,  $M$ ). That is, in practice one cannot additionally obtain a useful constraint on  $f$ . However, this limitation of KERRBB is handily overcome by pairing it with BHSPEC, which is based on non-LTE disk atmosphere models within an  $\alpha$ -viscosity prescription. BHSPEC has just two principal fit parameters (spin and mass accretion rate), and it can be used to fit directly for  $a_*$ . However, it does not include the effects of self-illumination of the disk (“returning radiation”), which is a feature that is included in KERRBB.

The pairing of KERRBB and BHSPEC is achieved using KERRBB2, which is a modified version of KERRBB that contains a pair of look-up tables for  $f$  corresponding to two values of the viscosity parameter:  $\alpha = 0.01$  and  $0.1$ . The entries in the tables are computed using BHSPEC. The two tables give  $f$  versus  $L/L_{\text{Edd}}$  for a wide range of the spin parameter ( $|a_*| \leq 0.9999$ ). The computations of  $f$  versus  $L/L_{\text{Edd}}$  are done using the appropriate, corresponding response matrices and energy ranges used in fitting the spectra with KERRBB. Thus, KERRBB and the subroutine/table computed using BHSPEC (which together constitute KERRBB2) allow one to fit directly for  $a_*$  and  $L/L_{\text{Edd}}$ , while retaining the returning-radiation feature of KERRBB.

Depending on the quality of a particular spectrum, it may be necessary to include minor spectral components (e.g., line or edge features), but these cosmetic features do not significantly affect the spin results. Typically, three model components are fitted in conjunction with the thermal component: a low-energy cutoff, a “reflected” component (e.g., Ross & Fabian 2007), and a Compton component. The cutoff is straightforward to model (e.g., Wilms et al. 2000), and the reflected component is relatively weak in disk-dominated spectra, even in the most extreme circumstances (Gou et al. 2011). It is the modeling of the Compton component that has been of central concern in applying the continuum-fitting method, and we discuss this issue now.

All spectra of black hole binaries, even the most disk-dominated, show a high-energy tail component of emission, which is widely attributed to Compton upscattering of soft photons by coronal electrons (Remillard & McClintock 2006). In early continuum-fitting work (Shafee et al. 2006; McClintock et al. 2006), this component was modeled unsatisfactorily by adding a power-law component to the spectrum. All subsequent work has used a much-improved empirical model of Comptonization called SIMPL (Steiner et al. 2009b). This model self-consistently generates the Compton component from the thermal seed spectrum of photons. It allows reliable measurements of spin to be obtained even as the fraction of seed photons  $f_{\text{SC}}$  that are scattered into the power-law component approaches 25% (Steiner et al. 2009a, 2009b). The use of SIMPL in place of the standard power law has doubled the body of useful data for several sources (e.g., see Steiner et al. 2011, 2012a), and it has enabled the measurement of

---

<sup>3</sup> For alternatives, see Gierliński et al. (2001), Kolehmainen & Done (2010), and Straub et al. (2011).



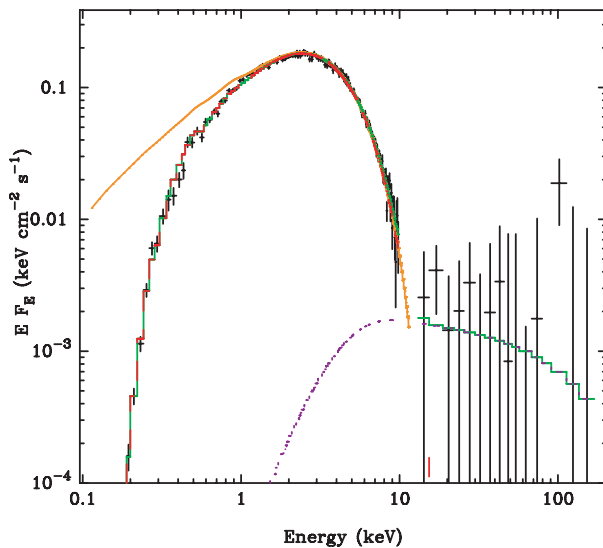


**Fig. 4** Model fit to a disk-dominated spectrum of LMC X-3 obtained using detectors aboard the *BeppoSAX* satellite for  $D = 52$  kpc,  $i = 67^\circ$  and  $M = 10 M_\odot$  (Davis et al. 2006). A green solid curve, which is difficult to discern because it hugs the data, is the total model. Also shown is the thermal component (red long-dashed curve) and the Compton component (violet short-dashed curve). The reflected component is negligible and was not included. The orange solid curve shows the total model with the effects of interstellar absorption removed. Note that the peak Compton flux is only 1% of the peak thermal flux.

the spins of black holes whose spectra are persistently quite strongly Comptonized such as LMC X-1 (Gou et al. 2009) and Cyg X-1 (Gou et al. 2011).

Successful application of the continuum-fitting method requires the selection of spectra that are disk-dominated. For transient sources, such spectra are typically observed during the latter part of an outburst cycle (Figure 2b). Figure 4 shows a spectrum with a peak flux in the Compton component that is only 1% of the peak thermal flux. For spectra that are this disk-dominated, how one chooses to model the adulterating Compton component is obviously quite unimportant. Meanwhile, there is an abundance of spectra of comparable quality available for several sources, i.e., sources with  $f_{\text{SC}} \sim 1\%$  (e.g., see Figure 1 in Steiner et al. 2009a, and Table 1 in Steiner et al. 2011).

While it is essential to select spectra that have a substantial thermal component (i.e.,  $f_{\text{SC}} \lesssim 25\%$ ; Steiner et al. 2009a), it is equally important to select data of moderate luminosity, specifically spectra with Eddington-scaled disk luminosities  $L/L_{\text{Edd}} < 0.3$ . Otherwise, the disk scale-height grows and the thin disk model is invalidated (Sections 4.2 and 5.2; McClintock et al. 2006). Fortunately, there is usually an abundance of such data because a typical transient source remains for months in a suitable disk-dominated state of moderate luminosity (see Figure 2b). A very wide range of detectors are capable of providing suitable data (see example in Section 4.1). The principal requirements are that the data can be corrected for dead time, and that the detector have a dozen or more energy channels, an appropriate bandwidth, and be well calibrated (Section 5.1).

#### 4 Truncation of the Disk at the ISCO

We review the large body of observational evidence that there exists a constant inner-disk radius in disk-dominated states of black hole binaries. We follow with theoretical evidence, based on GRMHD simulations, that this fixed radius can be identified with the radius of the ISCO.

#### 4.1 Observational Evidence

It has been clear for decades that fitting the X-ray continuum might prove to be a promising approach to measuring black hole spin. The earliest indications came with the advent in the mid-1980s of a nonrelativistic disk model (Mitsuda et al. 1984; Makishima et al. 1986), now referred to as DISKBB, which returns the color temperature  $T_{\text{in}}$  at the inner-disk radius  $R_{\text{in}}$ . In an important review paper, Tanaka & Lewin (1995) show the remarkable stability of  $R_{\text{in}}$  for three transients as the thermal flux of these sources steadily decays on a timescale of months by factors of 10–100 (see their Figure 3.14). Tanaka & Lewin remark that the constancy of  $R_{\text{in}}$  suggests that this fit parameter is related to the radius of the ISCO. Subsequently, similar evidence for a constant inner-disk radius in disk-dominated states of black hole binaries has been demonstrated for many sources by showing that the bolometric luminosity of the thermal component is approximately proportional to  $T_{\text{in}}^4$  (Kubota et al. 2001; Kubota & Makishima 2004; Gierliński & Done 2004; Abe et al. 2005; McClintock et al. 2009).

A recent study of the persistent source LMC X-3 presents the most compelling evidence to date for a constant inner-disk radius (Steiner et al. 2010). This result is based on an analysis of a large sample of X-ray spectra collected during eight X-ray missions that span 26 years. As illustrated in Figure 5 for a selected sample of 391 *RXTE* spectra, the radius of the accretion disk was found to be constant over time and unaffected by the gross variability of the source to within  $\approx 2$  percent. Even considering an ensemble of eight X-ray missions, the radius was observed to be stable to within  $\approx 5$  percent. These results provide compelling evidence for the existence of a fixed inner-disk radius and establish a firm empirical foundation for the measurement of black hole spin. The only reasonable inference is that this radius is closely associated with the radius of the ISCO, as we show to be the case in the following section.

#### 4.2 Theoretical Evidence

The NT model makes one key assumption: It assumes that the viscous torque vanishes inside the ISCO. While eminently reasonable (e.g., Paczyński 2000; Afshordi & Paczyński 2003; Shafee et al. 2008b), this “zero-torque” assumption does not follow directly from basic conservation laws but is applied as an extra ad hoc boundary condition. Furthermore, the luminosity profiles shown for the NT model in Figure 3b depend critically on this boundary condition because this condition causes the luminosity profiles to vanish at the ISCO, which in turn fixes the radius of peak disk emission. Krolik (1999) argued that magnetic stresses can operate freely across the ISCO and will cause strong torques at the ISCO, as well as in the inner plunging region. Also, Gammie (1999) came up with a simple analytical MHD model of the plunging region with demonstrably non-zero torques. What do real disks do?

To answer this question, geometrically thin accretion disks around black holes have been simulated by a number of authors (Shafee et al. 2008a; Noble & Krolik 2009; Penna et al. 2010) using state-of-the-art GRMHD codes. The main advantage of simulations is that they do not require ad hoc assumptions. One simply introduces magnetized gas in a Kerr space-time and lets the system evolve to a quasi-steady state. Since the ISCO lies inside the simulation box, well away from computational boundaries, it is not treated differently from other regions of the system. In other words, no boundary condition is applied by hand at the ISCO, a great improvement over analytical models.

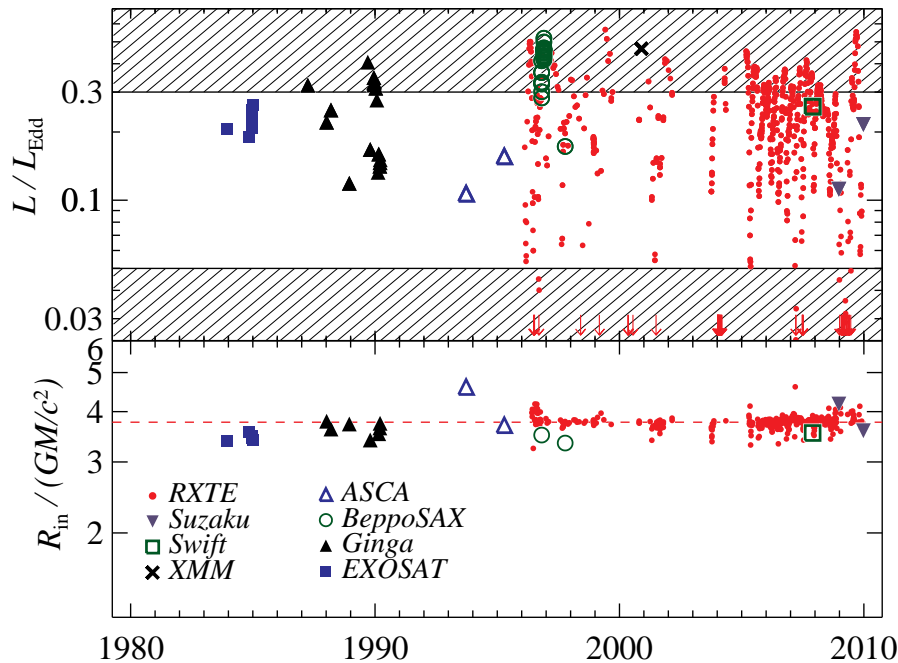


**Fig. 5** (*top*) Accretion disk luminosity in Eddington-scaled units (for  $M = 10 M_{\odot}$ ) versus time for all the 766 spectra considered in a study of LMC X-3 by Steiner et al. (2010). (Downward arrows indicate data that are off scale.) Selected data in the unshaded region satisfy the thin-disk selection criterion  $L/L_{\text{Edd}} < 0.3$  and avoid confusion with strongly-Comptonized hard-state data with  $f_{\text{SC}} \gtrsim 25\%$  (Section 3.2; Remillard & McClintock 2006). (*bottom*) Fitted values of the inner-disk radius are shown for thin-disk data in the top panel that meet the selection criteria of the study (a total of 411 spectra). Despite large variations in luminosity,  $r_{\text{in}}$  remains constant to within a few percent over time. The median value for just the 391 selected *RXTE* spectra is shown as a red dashed line.

On the other hand, for technical reasons, simulations to date have not treated radiation transfer self-consistently but instead have assumed local cooling. This is not considered serious for the purposes of testing the zero-torque condition.

The dashed lines in Figure 3b show results from simulations of very thin disks ( $H/R \sim 0.05$ ; Penna et al. 2010; Kulkarni et al. 2011; Zhu et al. 2012). The simulation-derived disk luminosity profiles show modest deviations from the NT model predictions; in particular, the disk flux does not vanish inside the ISCO. On the other hand, the deviations are minor, and we discuss and quantify these effects in Section 5.2. Importantly, the radius corresponding to the luminosity peak, which is the most relevant quantity for the continuum-fitting method, agrees quite well. As discussed in Section 5.2, the good agreement between model predictions and simulation results translates into modest uncertainties in spin estimates. GRMHD simulation results such as these shown in Figure 3b are viewed as a strong validation of the NT model.

Interestingly, the magnetic stress in the simulations does not vanish in the plunging region. Indeed, Penna et al. (2010) found that the stress there agrees remarkably well with Gammie’s (1999) model. However, there is little energy dissipation associated with

this stress (Gammie’s analytical model has zero dissipation), so it has little bearing on the continuum-fitting method. Another interesting result is that deviations from the NT model seem to increase as the luminosity and, concomitantly, the disk thickness increases<sup>4</sup> (Kulkarni et al. 2011), as anticipated in previous work (Paczynski 2000; Shafee et al. 2008b).

## 5 Uncertainties in Spin Estimates

The bottom line of this section is that the error in  $a_*$  is dominated by the observational errors in the external input parameters  $D$ ,  $i$  and  $M$ . By comparison, the errors due to reliance on the NT model, as well as on the disk atmosphere model that is used to correct for the effects of spectral hardening, are less important. Meanwhile, the one significant question that hangs over most of the spin results is the assumption that the black hole’s spin vector is aligned with the orbital angular momentum vector. We discuss these points in turn.

### 5.1 Observational Errors

In early work, the error in  $a_*$  attributable to the uncertainties in  $D$ ,  $i$  and  $M$  was only crudely estimated (Shafee et al. 2006; Davis et al. 2006; McClintock et al. 2006). However, in all subsequent work, starting with Liu et al. (2008), the error in the spin due to the combined uncertainties in these three parameters has been computed in detail via Monte Carlo simulations. That the error budget for  $a_*$  is dominated by the uncertainties in  $D$ ,  $i$  and  $M$  has been thoroughly demonstrated in recent work, which provides error estimates for a very wide range of statistical and systematic errors associated with (1) the details of the spectral models employed, (2) flux calibration uncertainties, (3) the effects of a warm absorber, etc. Instead of discussing such technical details here, we refer the reader to Section 5 and Appendix A in Steiner et al. (2011) and Section 5 in Gou et al. (2011).

### 5.2 Errors from the Novikov-Thorne Model

As described in Section 3.1, the NT model is robust and makes very few untested assumptions. It is true that some properties of the disk, e.g., the density and temperature of gas at the disk mid-plane, depend on the magnitude of the viscosity parameter  $\alpha$ , but the all-important luminosity profiles shown in Figure 3b do not. These profiles are a direct consequence of energy conservation – gas drifts inward, it converts gravitational potential energy into orbital kinetic and gas thermal energy, and the latter is radiated. This physics is independent of the value of  $\alpha$ , or even the validity of the  $\alpha$  prescription.

The NT model assumes that dissipated energy is radiated by the gas locally at the same radius. This is a very safe assumption. The cooling time of the gas in a thin accretion disk is approximately  $(H/R)^2$  times the viscous radial advection time. For

---

<sup>4</sup> In contrast, Noble et al. (2010) find that the stress profile is almost completely independent of disk thickness.

the disks of interest to the continuum-fitting method ( $H/R < 0.1$ ), this means that cooling is about 100 times faster than energy advection and hence very local.

Another approximation in the NT model is the neglect of disk self-irradiation. This is acceptable near the peak of the luminosity profile, where local energy dissipation greatly exceeds irradiation. However, it is less safe at larger radii. The models KERRBB and KERRBB2 (Section 3.2) include self-irradiation consistently. In practice, self-irradiation seems to have a minor effect on spin estimates.

As already discussed, the NT model assumes zero torque at the ISCO. Although this approximation turns out to be less severe than one might have anticipated (Figure 3b), we still expect it to have some effect on the continuum-fitting method. Several authors (Kulkarni et al. 2011; Noble et al. 2011; Zhu et al. 2012) have investigated this issue quantitatively. The general consensus is that the zero-torque approximation introduces uncertainties in spin estimates of around  $\Delta a_* \sim 0.1$  for low spin values  $a_* < 0.5$  and much smaller errors as  $a_* \rightarrow 1$ . For example, Kulkarni et al. (2011) estimate for  $a_* = 0, 0.7, 0.9$  and  $0.98$  that the respective values of  $\Delta a_*$  are 0.11, 0.06, 0.014 and 0.007. (Noble et al. 2011 estimate  $\Delta a_* \sim 0.2 - 0.3$  for  $a_* = 0$ .) These results are for a disk inclination angle of  $i = 60^\circ$  and a disk thickness of  $H/R = 0.05$ , which corresponds to  $L/L_{\text{Edd}} \sim 0.35$  (see Table 1 in Zhu et al. 2012). The errors are more severe for thicker disks. Meanwhile, the results quoted here are for the thinnest, lowest-luminosity disks simulated to date; presently, it is not practical to resolve the MRI turbulence in thinner disks.

Not only are these estimates of the NT model errors significantly less than the observational errors presented in Section 6, they are overestimates of the model errors because the continuum-fitting method is applied only to very thin disks: A strict requirement of the method is  $L/L_{\text{Edd}} < 0.3$ , while most measurements are based on spectral data with  $L/L_{\text{Edd}} \lesssim 0.1$ . Looking to the future, it might be possible to do better by replacing the NT model with a more accurate simulation-based model (e.g., Penna et al. 2012), but this step is not presently warranted. In conclusion, all continuum-fitting spin measurements published to date (see Section 6) are based on the NT model which systematically overestimates the spin; however, this source of error is presently small compared to the observational errors.

### 5.3 Errors from the Disk Atmosphere Model

An essential cornerstone of the continuum-fitting method is a reliable model of the disk's atmosphere. Such a model is BHSPEC (Davis & Hubeny 2006), which can be used either alone or including the effect of self-irradiation via KERRBB2. BHSPEC, which is quite sophisticated and includes a wide range of physical effects, is based on the non-LTE radiative transfer code TLUSTY (Hubeny & Lanz 1995), which was originally developed for stellar atmospheres.

At a given location on an accretion disk, BHSPEC computes the emitted spectrum using three supplied parameters: the effective temperature  $T_{\text{eff}}$  defined such that radiative flux  $F = \sigma T_{\text{eff}}^4$ , local vertical gravity parameter  $Q$ , and disk column density  $\Sigma$ . As discussed in previous sections, a robust estimate of  $T_{\text{eff}}$  can be obtained from the NT model, while the parameter  $Q$  is calculated directly from the Kerr metric. The main uncertainty is in the value of  $\Sigma$ .

In standard disk theory,  $\Sigma$  varies inversely as the viscosity parameter  $\alpha$  and is thus quite uncertain. Fortunately, in the case of optically thick disks (which all thermal state

disks are)  $\Sigma$  has only a weak effect on the emerging spectrum. This is analogous to the case of a star where the spectrum depends on the effective temperature and surface gravity, but not at all on the optical depth to the stellar core, which is effectively infinite. The optical depth through a disk is not quite infinite, hence there is some spectral dependence on  $\Sigma$ . However, this dependence is weak for models with  $L/L_{\text{Edd}} < 0.3$  (Davis & Hubeny 2006; Done & Davis 2008).

For the same reason, details of exactly how viscous heating is distributed vertically within the disk are unimportant. So long as energy dissipation occurs in the disk interior at optical depths greater than a few, the emerging spectrum depends only on  $T_{\text{eff}}$  and  $Q$  (Davis et al. 2005, 2009). This is not true if there is substantial energy dissipation close to or above the photosphere. Disks in the thermal state probably do not have such dissipation since their spectra show very little hard “coronal” emission (Remillard & McClintock 2006). Whatever little coronal emission is present is fitted for via a model for the Compton power law such as SIMPL (Section 3.2).

The standard BHSPEC model assumes hydrostatic equilibrium and does not include the force from magnetic fields. However, numerical simulations (e.g., Hirose et al. 2009) indicate that the photospheric surface regions show modest deviations from hydrostatic equilibrium and are primarily supported by magnetic forces. Including these effects in BHSPEC generally leads to a modest ( $< 10\%$ ) increase in the spectral hardness (Davis et al. 2009). The effects of irradiation (both self- and from a corona), which have not yet been rigorously explored, may also lead to a slight hardening of the spectrum. In summary, while there are uncertainties associated with the disk spectral model used in the continuum-fitting method, it appears unlikely that the resulting errors in  $R_{\text{in}}$  are more than 10%, which for low values of spin implies  $\Delta a_* \sim 0.1$ , decreasing as  $a_* \rightarrow 1$  (Figure 3a).

#### 5.4 Assumption of Spin-Orbit Alignment

In determining the spins of eight of the ten black holes (see Section 6), it is assumed that the plane of the inner X-ray-emitting portion of the disk is aligned with the binary orbital plane, whose inclination angle  $i$  is determined from optical observations (e.g., Orosz et al. 2011a). However, if a black hole’s spin is misaligned with the orbital vector, this will warp a thin disk because the Bardeen-Petterson effect will force the inner disk to align with the black hole spin vector (Bardeen & Petterson 1975)<sup>5</sup>. An error in estimating the inclination of the inner disk of  $\sim 10^\circ$  or more, resulting from an erroneous use of  $i$  as a proxy for the inclination of the inner disk, would substantially corrupt most continuum-fitting measurements of spin<sup>6</sup>.

There is evidence for gross spin-orbit misalignment for one transient system (SAX J1819.3-2525); however, this evidence is weak (Narayan & McClintock 2005). For the transients generally, more recent evidence, which is summarized in Section 1 of Steiner & McClintock (2012), argues in favor of alignment. Briefly, the timescale for accretion to torque the black hole into alignment is estimated to be  $\sim 10^6 - 10^8$  years, which is short compared to the typical lifetime of a transient system (Section 2.2). In the case of the persistent supergiant systems, there is some evidence that their more massive black

<sup>5</sup> While thin disks are subject to warping, thick disks are not (Dexter & Fragile 2011).

<sup>6</sup> Unfortunately the continuum-fitting method cannot fit for the inclination of the inner disk because there is a degeneracy between the inclination and spin parameter (Li et al. 2009).

holes are formed by direct, kickless collapse (Mirabel & Rodrigues 2003; Reid et al. 2011). Finally, a population synthesis study based on a maximally conservative (i.e., minimum-torque) assumption indicates that the spin axes of most black hole primaries will be tilted less than  $10^\circ$  (Fragos et al. 2010).

In determining the spins of the remaining two black holes (see Section 6), the inclination of the inner disk is taken to be the inclination  $\theta$  of the radio or X-ray jet axis, which is presumed to be aligned with the black hole’s spin axis. The jet inclination angle for these microquasars, GRS 1915+105 and H1743–322, was determined by modeling proper-motion data derived from radio and X-ray observations (Mirabel & Rodríguez 1994; Fender et al. 1999; Steiner et al. 2012a). Fortunately, radio/X-ray jet data have also yielded a strong constraint on  $\theta$  for a third microquasar, XTE J1550–564, thereby providing a rare opportunity to check directly the assumption of spin orbit alignment because its orbital inclination angle  $i$  has also been measured (Orosz et al. 2011b). In this case, Steiner & McClintock (2012) find no evidence for misalignment and place an upper limit on the difference between the spin and orbital inclinations of  $|\theta - i| < 12$  deg (90% confidence).

## 6 Results and Discussion

Table 1 lists the masses and spins of ten stellar black holes. By virtue of the no-hair theorem, this table provides complete descriptions of each of these ten black holes. The spins span the full range of prograde values, and the masses range from 6 to  $16 M_\odot$ . In addition to the continuum-fitting spin data in Table 1, Gierliński et al. (2001) provide preliminary estimates for the spins of LMC X-1 and GRO J1655–50, Kolehmainen & Done (2010) report a hard upper limit of  $a_* < 0.9$  on the spin of GX 339–4, and Nowak et al. (2012) argue that the spin of 4U 1957+11 is extreme. Concerning 4U 1957+11, it is unclear if the compact object is a black hole, and the key parameters  $D$  and  $M$  are essentially unconstrained. Finally, Middleton et al. (2006) find an apparently moderate value of spin for GRS 1915+105, which is at odds with the extreme value in Table 1; Middleton et al. obtained a depressed value of spin because they relied on high-luminosity data, as explained in Section 5.3 in McClintock et al. (2006).

Caution is required in considering the errors for the values of spin quoted in Table 1 assuming that they are Gaussian, particularly for  $a_* \gtrsim 0.7$ . Note in Figure 3a how insensitive  $a_*$  is to large changes in the observable  $R_{\text{ISCO}}$  as  $a_*$  approaches unity. As a consequence of this limiting behavior of  $a_*$ , doubling a  $1\sigma$  error to approximate a  $2\sigma$  error can lead to nonsense. For example, formally increasing the nominal spin of LMC X-1 ( $a_* = 0.92$ ; Table 1) by doubling the  $1\sigma$  error ( $\Delta a_* = 0.05$ ) implies a  $2\sigma$  upper limit of  $a_* < 1.02$ , whereas the correct  $2\sigma$  upper limit is  $a_* < 0.98$  (see Figure 8 in Gou et al. 2009).

### 6.1 The Persistent Systems vs. the Transients

There is a dichotomy between the black holes in persistent systems and those in transients, both in their masses and their spins (Table 1). Considering spin first, the three persistent black holes all have high or extreme spins. In contrast, the spins of the transient black holes range widely: Four have spins consistent with zero, two have

**Table 1** The masses and spins, measured via continuum-fitting, of ten stellar black holes<sup>a</sup>.

System	$a_*$	$M/M_\odot$	References
Persistent			
Cyg X-1	$> 0.95$	$14.8 \pm 1.0$	Gou et al. 2011; Orosz et al. 2011a
LMC X-1	$0.92_{-0.07}^{+0.05}$	$10.9 \pm 1.4$	Gou et al. 2009; Orosz et al. 2009
M33 X-7	$0.84 \pm 0.05$	$15.65 \pm 1.45$	Liu et al. 2008; Orosz et al. 2007
Transient			
GRS 1915+105	$> 0.95^b$	$10.1 \pm 0.6$	McClintock et al. 2006; Steeghs et al. 2013
4U 1543–47	$0.80 \pm 0.10^b$	$9.4 \pm 1.0$	Shafee et al. 2006; Orosz 2003
GRO J1655–40	$0.70 \pm 0.10^b$	$6.3 \pm 0.5$	Shafee et al. 2006; Greene et al. 2001
XTE J1550–564	$0.34_{-0.28}^{+0.20}$	$9.1 \pm 0.6$	Steiner et al. 2011; Orosz et al. 2011b
H1743–322	$0.2 \pm 0.3$	$\sim 8^c$	Steiner et al. 2012a
LMC X-3	$< 0.3^d$	$7.6 \pm 1.6$	Davis et al. 2006; Orosz 2003
A0620–00	$0.12 \pm 0.19$	$6.6 \pm 0.25$	Gou et al. 2010; Cantrell et al. 2010

Notes:

<sup>a</sup> Errors are quoted at the 68% level of confidence, except for the three spin limits, which are estimated to be at the 99.7% level of confidence.

<sup>b</sup> Uncertainties greater than those in papers cited because early error estimates were crude.

<sup>c</sup> Mass estimated using an empirical mass distribution (Özel et al. 2010).

<sup>d</sup> Preliminary result pending improved measurements of  $M$  and  $i$ .

intermediate values of spin, and one is a near-extreme Kerr hole. The dichotomy is sharpened if one considers six additional transient black holes all of whose spins are predicted to be  $a_* \lesssim 0.8$  (Steiner et al. 2013) based on a fitted correlation between radio power and spin (Section 7.2).

Not only are the persistent black holes rapidly spinning, they are also massive – 11 – 16  $M_\odot$  – compared to the transient black holes. The masses of the transients are significantly lower and, remarkably, their mass distribution is narrow:  $7.8 \pm 1.2 M_\odot$  (Özel et al. 2010; Farr et al. 2011).

## 6.2 Prograde Spins that obey the Kerr Bound

The lack of negative spins in Table 1 may be the result, in a close binary system, of the expected alignment of the spin of the black hole progenitor with the orbital angular momentum, and it may also indicate that black hole kicks are not strong enough to flip the black hole into a retrograde configuration. While interesting that there are no negative spins, it is equally interesting that the spins of all ten black holes obey the Kerr bound  $|a_*| < 1$ . In particular, if the distances to either Cyg X-1 or GRS 1915+105 were  $\sim 30\%$  less than the best current estimates, then it would be impossible to fit the data with the KERRBB2 model, which only accommodates spin values  $a_* < 1$ . Because the observed values of each of the three external fit parameters ( $D$ ,  $i$  and  $M$ ) place hard constraints when fitting the data, a failure to fit a spectrum that requires  $a_* > 1$  has the potential to falsify the spin model. For a discussion of this point in relation to the near-extreme Kerr hole GRS 1915+105, see Section 6.4 in McClintock et al. (2006).



### 6.3 The High Natal Spins of the Persistent Black Holes

It is reasonable to conclude that the black holes in the persistent systems were born with high spins because their host systems are too young for these black holes to have been spun up by accretion torques. Consider, for example, the persistent system Cyg X-1 (Gou et al. 2011): For its black hole to achieve its present spin of  $a_* > 0.95$  via disk accretion, an initially nonspinning black hole would have had to accrete  $> 7.3 M_\odot$  from its donor (Bardeen 1970; King & Kolb 1999) to become the  $14.8 M_\odot$  black hole we observe today. However, even at the maximum (Eddington-limited) accretion rate this would require  $> 31$  million years, while the age of the system is between 4.8 and 7.6 million years (Wong et al. 2012). Likewise for M33 X-7 and LMC X-1, the corresponding minimum spin-up timescales are  $> 17$  and  $> 25$  million years, respectively, while the respective ages of the systems are  $\lesssim 3$  and  $\lesssim 5$  million years (Gou et al. 2011). It therefore appears that the spins of these systems must be chiefly natal, although possibly such high spins could be achieved during a short-lived evolutionary phase of hypercritical accretion (Moreno Méndez et al. 2008).

### 6.4 Applications

The data in Table 1 have a number of applications to physics and astrophysics, both immediate and potential. In physics, a high goal is to use such data as a springboard to test the no-hair theorem (see Section 8), and the foundation for any such test is high-quality measurements of mass and spin for a good sample of black holes. In astrophysics, knowledge of the spins of stellar black holes is crucial for example in constraining models of gamma-ray burst sources (Woosley 1993; MacFadyen & Woosley 1999; Woosley & Heger 2006); supernovae and black hole formation (Lee et al. 2002; Wong et al. 2012); exotic black hole states and state transitions (Remillard & McClintock 2006); and in informing LIGO/VIRGO modelers who are computing gravitational-wave signals (Campanelli et al. 2006). A central question, which we turn to in the next section, is the role of spin in powering jets.

## 7 Jet Power and Black Hole Spin

Since the spin parameter  $a_*$  is one of only two numbers that completely characterize a black hole (mass  $M$  being the other), it stands to reason that it should influence at least some observational properties of the hole. The most widely discussed connection is to relativistic jets.

The story goes back to Penrose (1969) who showed that a spinning black hole has free energy that can in principle be tapped by specially prepared infalling particles. Although Penrose's specific proposal is not considered promising, the idea of extracting energy from spinning black holes has stuck and has become popular in astrophysics. Ruffini & Wilson (1975, see also Damour et al. 1978) and Blandford & Znajek (1977) suggested a specific mechanism whereby a force-free poloidal magnetic field around a spinning black hole is twisted by frame dragging, thereby producing outgoing Poynting flux along twin jets. We refer to this as the generalized Penrose process.

GRMHD simulations of accreting black holes have found MHD jets forming spontaneously from generic initial conditions (e.g., Koide et al. 2002; McKinney & Gammie

2004; McKinney 2005; Beckwith et al. 2008; McKinney & Blandford 2009). Moreover, in one particular simulation involving a rapidly spinning black hole and a strong poloidal field, Tchekhovskoy et al. (2011) showed that the power carried by the jet exceeded the total rest mass energy of accreted gas, meaning that the jet extracted energy from the spinning black hole.

On the observational front, until recently there was no empirical evidence for a connection between black hole spin and relativistic jets. We discuss here the first such evidence.

### 7.1 Two Kinds of Jets in Black Hole Binaries

Fender et al. (2004) identified a number of systematic properties in the radio emission of black hole binary jets. They showed that there are two kinds of jets, which we refer to as “steady jets” and “ballistic jets,” each associated with a specific spectral state of the X-ray source. Although we discuss both kinds of jets for completeness, our focus here is on the ballistic jet.

The steady jet is observed as a continuous outflow of plasma in the hard spectral state (for a discussion of spectral states in black hole binaries, see Remillard & McClintock 2006). This jet is small-scale, being observable only out to a few tens of AU, and it appears not to be very relativistic. It is present at the very start of a transient’s outburst cycle. Referring to the X-ray light curves for XTE J1859+226 in Figure 2a, the jet is present during the first few days when the hard flux (panel a) is most intense and the 2–12 keV flux (panel b) is increasing rapidly. It then disappears, and it returns only near the end of the outburst cycle (beyond the right edge of the plot). The steady jet is seen in all transients at low values of  $\dot{M}$ .

The far more dramatic ballistic jet is launched when a transient goes into outburst (Fender et al. 2004). This powerful transient jet usually appears near (or soon after) the time of outburst maximum, as the source switches from its initial hard state to a soft state via the “steep power-law” state. Ballistic jets manifest themselves as blobs of radio (and occasionally X-ray) emitting plasma that move ballistically outward at relativistic speeds (Lorentz factor  $\Gamma > 2$ ). They are often observed out to distances of order a parsec. Because ballistic jets resemble the kpc-scale jets seen in quasars, black hole binaries that produce them are called microquasars (Mirabel & Rodríguez 1999).

Ballistic jet ejection occurs at a very specific stage during the spectral evolution of a given system (Fender et al. 2004). In Figure 2, the strong spike in the radio light curve (panel d), which is characteristically delayed relative to the corresponding spike in the X-ray luminosity (panel b), is associated with a ballistic jet. As most clearly demonstrated for the prototypical microquasar GRS 1915+105 (Fender & Belloni 2004), this ejection stage appears to correspond to the inward-moving inner edge of the accretion disk reaching the ISCO, which apparently results in some violent event that launches a large-scale relativistic blob.

On general principles, one expects jet power to depend on a black hole’s mass  $M$  and spin  $a_*$ , and the mass accretion rate  $\dot{M}$ , plus other factors such as the strength and topology of the magnetic field. If one wishes to investigate the dependence of jet power on  $a_*$ , one needs first to eliminate the other variables.

For steady jets,  $\dot{M}$  spans a wide range, and it is not straightforward to eliminate the effects of this variable. It is possible to do this, however, by using the disk X-ray luminosity as a proxy for  $\dot{M}$  (e.g., Heinz & Sunyaev 2003; Merloni et al. 2003; Falcke et al.

2004; Fender et al. 2004; Fender & Belloni 2004), but one must have knowledge of the radiative efficiency of the disk, which is generally both low and variable in the hard state where the steady jet forms (see Narayan & McClintock 2008, for a discussion of radiatively inefficient accretion in the hard state). The procedure is relatively uncertain and it is difficult to obtain robust results. Nevertheless, Fender et al. (2004) have performed such a study and have claimed that there is no evidence in the data that the power of a steady jet depends on spin.

Ballistic jets on the other hand invariably occur near the peak of transient outbursts. Steiner et al. (2013) have shown that during major outbursts the peak disk luminosities in various transients are near the Eddington limit and are clustered within a factor of  $\sim 2$  in luminosity, which means that these systems behave for all purposes like “standard candles.” This crucially allows one to compare the power of ballistic jets observed for different black holes at the same  $\dot{M}$ , namely  $\dot{M} \sim \dot{M}_{\text{Edd}}$ . In addition, all black holes in transients have similar masses to better than a factor of two (Özel et al. 2010); furthermore, it is easy to correct for any mass dependence (see below). This leaves  $a_*$  (with magnetic field as a wild card) as the sole remaining parameter that could have any influence on jet power.

Let us define the jet efficiency factor  $\eta$  of a ballistic jet,

$$\eta_{\text{jet}}(a_*) = \langle L_{\text{jet}} \rangle / \langle \dot{M} \rangle c^2, \quad (1)$$

where  $\langle L_{\text{jet}} \rangle$  is the time-average kinetic luminosity flowing out through the jet and  $\langle \dot{M} \rangle c^2$  is the time-average rate at which rest-mass energy flows into the black hole. Using (1) radio luminosity as a proxy for  $L_{\text{jet}}$  (Narayan & McClintock 2012) and (2) observed values for the peak radio luminosities for five black holes that are all accreting at  $\sim \dot{M}_{\text{Edd}}$  (Steiner et al. 2013), one can infer directly how jet luminosity depends on spin, as we discuss in the following section.

## 7.2 Correlation Between Spin and Ballistic Jet Power

A typical ballistic jet blob is initially optically thick and has a low radio power. As the blob moves out and expands, the larger surface area causes its radio power to increase. This continues until the blob becomes optically thin, after which the flux declines rapidly. The overall behavior is generally consistent with an expanding conical jet (van der Laan 1966; Hjellming & Johnston 1988). Moreover, as discussed in Section 7.4.3, the peak radio luminosity is expected to scale more or less linearly with the jet kinetic energy or kinetic luminosity. Thus, peak radio luminosity is a good proxy for jet kinetic luminosity.

Narayan & McClintock (2012) considered the peak radio luminosities of ballistic jet blobs in four transients, A0620–00, XTE J1550–564, GRO J1655–40, GRS 1915+105, and showed that they correlated well with the corresponding black hole spins measured via the continuum-fitting method<sup>7</sup>. Later, Steiner et al. (2013) included a fifth transient, H1743–322, whose spin had been just measured. Figure 6a shows a plot of the black hole spins of these five objects versus a measured quantity called “Jet Power,”

<sup>7</sup> In the case of a fifth transient, 4U1543–47, radio observations did not include the peak of the light curve, so one could only deduce a lower limit to the jet power. Note that the radio peak can be very narrow in time, e.g.,  $\approx 1$ -day in the case of XTE J1859+226 (Figure 2), so one requires dense radio monitoring to catch the peak.

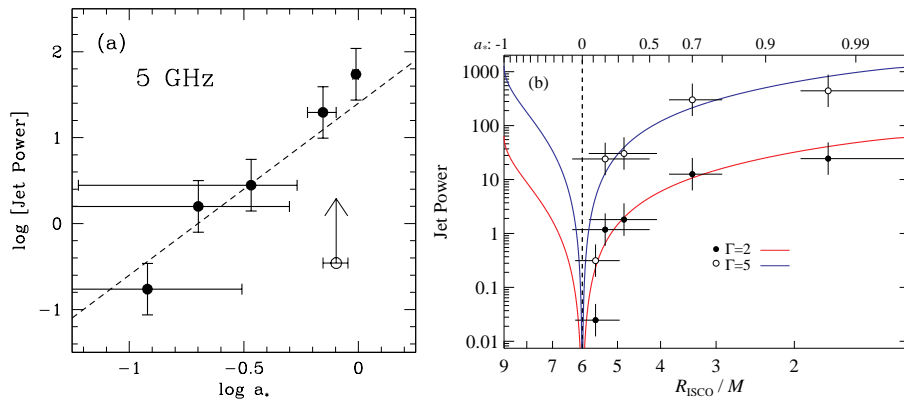


**Fig. 6** (a) Plot of the quantity Jet Power, which measures the 5 GHz radio luminosity at light curve maximum, versus black hole spin, measured via the continuum-fitting method for five transients (Narayan & McClintock 2012; Steiner et al. 2013). The dashed line has slope equal to 2. (b) Plot of Jet Power versus  $R_{\text{ISCO}}/(GM/c^2)$ . Here the radio luminosity has been corrected for beaming assuming a bulk Lorentz factor  $\Gamma = 2$  (filled circles) or  $\Gamma = 5$  (open circles). The solid lines correspond to Jet Power  $\propto \Omega_{\text{H}}^2$ , where  $\Omega_{\text{H}}$  is the angular frequency of the horizon (Steiner et al. 2013).

which refers to the radio luminosity  $\nu L_{\nu} = (\nu S_{\nu})D^2/M$  (here, not corrected for beaming), where  $\nu = 5$  GHz is the radio frequency,  $S_{\nu}$  is the flux density in Jy at the peak of the ballistic-jet radio light curve,  $D$  is the distance in kpc, and  $M$  is the black hole mass in solar units<sup>8</sup>. That is, the proxy adopted for jet kinetic luminosity is simply the peak radio luminosity at 5 GHz<sup>9</sup>. Figure 6a shows unmistakable evidence for a strong correlation between Jet Power and  $a_*$ . Note that Jet Power varies by nearly three orders of magnitude as the spin parameter varies from  $\approx 0.1 - 1$ .

The uncertainty in the estimated values of Jet Power, which is difficult to assess, is arbitrarily and uniformly assumed to be a factor of two (Narayan & McClintock 2012). The very unequal horizontal error bars in Figure 6a are a feature of the continuum-fitting method of measuring  $a_*$ . Recall that the method in effect measures  $R_{\text{ISCO}}$  and then deduces the value of  $a_*$  using the mapping shown in Figure 3a. Since the mapping is highly non-linear, especially as  $a_* \rightarrow 1$ , comparable errors in  $R_{\text{ISCO}}$  correspond to vastly different uncertainties in  $a_*$ . In addition, the use of  $\log a_*$  along the horizontal axis tends to stretch error bars excessively for low spin values. This point is clarified by considering Figure 6b, based on Steiner et al. (2013). Here the horizontal axis tracks  $\log R_{\text{ISCO}}$  rather than  $\log a_*$ , and the horizontal error bars are therefore more nearly equal. The key point is, regardless of how one plots the data, the correlation between Jet Power and black hole spin appears to be strong.

<sup>8</sup> The scaling by mass is sensible because the sources are near the Eddington luminosity limit, which is proportional to mass. However, since the masses of the black holes differ little (Table 1), the results would be virtually identical if the mass scaling were eliminated.

<sup>9</sup> None of the results change if one chooses a different reference frequency, e.g., 1.4 GHz or 15 GHz.

### 7.3 What Does it Mean?

Assuming the correlation shown in Figure 6 is real, there are two immediate implications: (i) Ballistic jets in black hole binaries are highly sensitive to the spins of their underlying black holes, presumably because these jets derive their power directly from the spin energy of the hole (à la Penrose 1969; Ruffini & Wilson 1975; Blandford & Znajek 1977). (ii) Spin estimates of stellar black holes obtained via the continuum-fitting method are sufficiently reliable to reveal this long-sought connection between relativistic jets and black hole spin.

With respect to item (i), we note that the mere existence of a correlation does not necessarily imply that the Penrose process is at work. We know that the gravitational potential in the inner disk deepens with increasing black hole spin, since the inner radius of the disk ( $R_{\text{ISCO}}$ ) shrinks with increasing  $a_*$  (Figure 3a).

Could this disk-related effect be the reason for the increasing jet power? It seems unlikely. The radiative efficiency of a Novikov-Thorne thin accretion disk increases only modestly with spin; for the five objects shown in Figure 6, the radiative efficiencies are 0.061, 0.069, 0.072, 0.10 and 0.19, respectively, varying by a factor of  $\approx 3$ . It seems implausible that a disk-powered jet could vary in radio Jet Power by the orders of magnitude seen in Figure 6.

In contrast, any mechanism that taps directly into the black hole spin energy via something like the Penrose process can easily account for the observed large variation in Jet Power. For instance, the generalized Penrose effect predicts that the jet efficiency factor should vary as  $\eta_{\text{jet}} \propto a_*^2$  (Ruffini & Wilson 1975; Blandford & Znajek 1977) or, more precisely, as  $\eta_{\text{jet}} \propto \Omega_{\text{H}}^2$  (Tchekhovskoy et al. 2010), where  $\Omega_{\text{H}}$  is the angular frequency of the black hole horizon<sup>10</sup>,

$$\Omega_{\text{H}} = \frac{c^3}{2GM} \left( \frac{a_*}{1 + \sqrt{1 - a_*^2}} \right). \quad (2)$$

The dashed line in Figure 6a corresponds to Jet Power  $\propto a_*^2$  and the solid lines in Figure 6b to  $\propto \Omega_{\text{H}}^2$ . The observational data agree remarkably well with these scalings, strongly suggesting that a Penrose-like process is in operation.

While the above conclusions are highly satisfying, one should not discount other possibilities. First, the correlation shown in Figure 6 is based on only five objects. Although this is mitigated by the very wide range of Jet Powers, the correlation might become weaker with the next spin measurement. Second, the correlation might arise if Jet Power and spin are each correlated with some third parameter. For instance, it is intriguing that the binary orbital periods of the five transients under consideration increase systematically with Jet Power. One could imagine scenarios in which the energy of ejected blobs depends on the size of the accretion disk, which depends in turn on the orbital period. However, it is less easy to see why the values of  $a_*$  measured with the continuum-fitting method should correlate with the orbital period, while conspiring to produce the scaling predicted by Blandford & Znajek (1977).

Returning to the subject of steady jets, it is interesting to consider why there is apparently no correlation between jet radio luminosity and spin (Fender et al. 2010; Russell et al. 2013). One likely answer is that steady jets and ballistic jets are produced via very different mechanisms. Perhaps ballistic jets are launched within a

<sup>10</sup> The two scalings agree for small values of  $a_*$ , but differ as  $a_* \rightarrow 1$ .

few gravitational radii, near  $R_{\text{ISCO}}$ , where the black hole spin could plausibly have a strong effect, whereas steady jets in the hard state originate much further out at radii  $\sim 10 - 100 \text{ GM}/c^2$  (e.g., Markoff et al. 2005), where the effects of spin are relatively weak. In support of this explanation, ballistic jets are definitely relativistic, with Lorentz factors of up to several (Fender et al. 2004, 2006), whereas there is little evidence that steady jets are relativistic (Gallo et al. 2003; Narayan & McClintock 2005).

#### 7.4 A Challenge

Based on an analysis of a heterogeneous data sample of uneven quality, Fender et al. (2010) claim that there is no evidence for a correlation between the power of ballistic jets and black hole spin. The substantial difference between the results obtained by these authors and Narayan & McClintock (2012) is, in the end, determined by the quantity used to represent jet power (which is discussed further in Section 7.4.3). Fender et al. compute jet power from the peak radio luminosity and rise time of a particular synchrotron event; adopt a formula relating jet power to X-ray luminosity, namely,  $\log_{10} L_{\text{jet}} = c + 0.5(\log_{10} L_x - 34)$ ; and use the normalization constant  $c$  as their proxy for the jet power. Narayan and McClintock, on the other hand, use the model-independent proxy discussed above, namely, the maximum observed radio luminosity at 5 GHz.

Very recently, the three authors of Fender et al. (2010) have written a second paper (Russell et al. 2013) repeating their claim that there is no evidence for a correlation between the power of ballistic jets and black hole spin. Therein, they challenge the methodologies and findings of Narayan & McClintock (2012) and Steiner et al. (2013). A response to this challenge is being readied (J. Steiner et al., in preparation); meantime, the following is a preliminary sketch of the elements of this response. The following comments pertain only to ballistic jets and continuum-fitting spin measurements. (Russell et al. 2013, also discuss steady jets and Fe-line spin measurements).

##### 7.4.1 Significance of the Result

Russell et al. (2013) contend that the empirical correlation shown in Figure 6a is only marginally statistically significant ( $\approx 90\%$  confidence). Their analysis is based on a Bayesian linear regression model (Kelly 2007), which incorporates an additional parameter that allows for intrinsic noise; this putative and undefined source of noise is distinct from measurement error. Adopting precisely the procedures of Russell et al., but using the Steiner et al. (2013) data set, we confirm the correlation at  $\approx 95\%$  confidence<sup>11</sup>. In contrast, a traditional analysis (i.e., a linear fit using two-dimensional error bars) produces a correlation at  $\approx 99.9\%$  confidence. A comparably strong result is achieved using the Kelly (2007) model if one applies the usual Jeffreys noninformative prior to the intrinsic noise term rather than the default flat prior, which preferentially selects solutions corresponding to large estimates of intrinsic noise.

<sup>11</sup> The lower level of confidence reported by Russell et al. (2013) is largely attributable to their use of radio data for a flare of H1743–322 that is unrelated to the ballistic jet, namely a flare event that occurred 28 days before the X-ray flux peaked (McClintock et al. 2009). We focus solely on post-Eddington radio flares. The relevant radio flare event, which we consider, occurred 2.6 days after X-ray maximum (Steiner et al. 2013).

Of greater importance, Russell et al. (2013) consider only the empirical correlation shown in Figure 6a, and they disregard the physical model which takes into account beaming effects, namely, the model shown in Figure 6b. The application of this physical model is based on four simple assumptions: (i) spin-orbit alignment (Steiner & McClintock 2012); (ii)  $\Gamma$  is the same for all five sources and bracketed between 2 and 5 (Fender 2006); (iii) jet power is proportional to  $\Omega_{\text{H}}^2$  (Blandford & Znajek 1977; Tchekhovskoy et al. 2010); and (iv) radio luminosity can be used as a proxy for jet power (Sections 7.2 and 7.4.3). Fitting the Steiner et al. (2013) data set to this model, with the model normalization as its *sole* fit parameter, one obtains good fits (shown in Figure 6b) with  $\chi^2/\nu = 0.3$  and  $0.5$  for  $\Gamma = 2$  and  $5$ , respectively. This relationship is determined over a span of  $\sim 3$  orders of magnitude in jet power, and over the full allowed range of prograde spins. It is reasonable to view this result as evidence that the Blandford-Znajek model successfully describes the behavior of a ballistic jet produced by a black hole transient as it approaches its Eddington limit.

#### 7.4.2 Issue of Data Selection

Russell et al. (2013) furthermore argue that Narayan & McClintock (2012) and Steiner et al. (2013) omit data for several systems that should be included in the correlation plots shown in Figure 6. These additional data, which are plotted in Figure 1c in Russell et al. (2013), destroy the clean correlation shown in Figure 6a. However, it is inappropriate to include these data, and we reject them for the following reasons.

**Cygnus X-1** radiates persistently at a few percent of Eddington and, during its periods of jet ejection (Fender et al. 2006), its mass accretion rate is both very low and poorly constrained. At the same time, as stressed in Section 7.1, comparing sources at the same mass accretion rate, namely  $\dot{M} \sim \dot{M}_{\text{Edd}}$ , is the essential methodological requirement that eliminates the otherwise unknown dependency of the jet efficiency  $\eta_{\text{jet}}$  on  $\dot{M}$  (see equation 1). In order to include Cyg X-1 in the Steiner et al. (2013) sample, it would be necessary to know the precise scaling of jet power with  $\dot{M}$  and then to estimate  $\dot{M}$  at the time of jet ejection;  $\dot{M}$  is  $\sim 1 - 2$  orders of magnitude below Eddington and highly uncertain. Russell et al. (2013) ignore this problem.

For **GRS 1124-68** and **GS 2000+25**, Russell et al. (2013) adopt continuum-fitting spin data that are completely unreliable. These data are from a pioneering, proof-of-concept paper on continuum fitting (Zhang et al. 1997) whose authors note that the crucial “system parameters [i.e.,  $D$ ,  $i$  and  $M$ ] are mostly unknown.” More importantly, the values of spin adopted by Russell et al. for these two sources were simply inferred by Zhang et al. from crude estimates of the inner-disk radius  $R_{\text{in}}$  taken from a review paper (Tanaka & Lewin 1995); these estimates of  $R_{\text{in}}$  were, moreover, computed using the nonrelativistic disk model DISKBB that assumes a grossly incorrect inner-boundary condition (Zimmerman et al. 2005), while neglecting the effects of spectral hardening.

**GRS J1655-40** had major outbursts in both 1994 and 2005. Russell et al. (2013) plot in their Figure 1c a data point for the 2005 outburst which corresponds to a very faint radio flare. Narayan & McClintock (2012) and Steiner et al. (2013) do not include data for the 2005 outburst in their sample because the radio coverage was too sparse: The proximate observations that bracket the peak 4.3 Crab flare (see RXTE/ASM plot in Figure 1 in Brocksopp et al. 2006) occur 2.3 days before and 4.7 days after the 2-12 keV maximum (see observation log in the NRAO VLA archive and web link to a plot of the radio data in Rupen et al. 2005). We argue that the source produced a bright and brief radio flare (e.g., like the 1-day radio spike observed for XTE J1859+226

shown in Figure 2d), which was not observed because of the week-long gap in radio coverage. For the 2002 outburst of 4U 1543–47, we likewise hold that the radio coverage was inadequate and the radio flare was missed, as discussed in Narayan & McClintock (2012).

### 7.4.3 Synchrotron Bubble Model

Another point of contention is how to relate the radio luminosity  $\nu L_\nu$  observed at the peak of the light curve — this is the quantity “Jet Power” in Figure 6 — to physical conditions in the jet. Steiner et al. (2013) used synchrotron theory with the following standard assumptions: (1) The nonthermal radio-emitting electrons in the jet blob have an energy distribution  $N(\gamma) \sim \gamma^{-p}$  where  $\gamma$  is the electron Lorentz factor in the blob frame; (2)  $p = 5/2$  to be consistent with the synchrotron spectrum; (3) the magnetic energy in the blob is in equipartition with the energy in the nonthermal electrons; (4) there is one proton for each nonthermal electron and the total energy of the blob is dominated by the kinetic energy  $E$  of the protons; and (5) at light curve maximum, the jet blob transitions from optically thick to thin (van der Laan 1966). Steiner et al. showed that  $E \sim (\nu L_\nu)^{1.2}$ , i.e., the blob energy varies approximately linearly with  $\nu L_\nu$ . They thus argued that the latter is a good proxy for the former.

Why consider blob energy  $E$ ? In the synchrotron bubble model (van der Laan 1966), the jet ejection is some brief episode that is not observationally resolved. Hence the total ejected energy is all that one can measure. Russell et al. (2013) (and references therein) focus on the jet kinetic luminosity,  $L_{\text{jet}} = dE/dt \sim E/t_{\text{jet}}$ , where  $t_{\text{jet}}$  is the duration of the jet ejection. They further assume that the jet is ejected continuously, with a constant luminosity, until light curve maximum<sup>12</sup>. How does  $L_{\text{jet}}$  depend on  $\nu L_\nu$ ? Steiner et al. (2013) find that the radius of the jet blob scales as  $R \sim (\nu L_\nu)^{0.5}$ . Therefore, if the blob expands with some constant speed, say  $c$ , then  $L_{\text{jet}} \sim E/(R/c) \sim (\nu L_\nu)^{0.7}$ , i.e., jet kinetic luminosity varies as  $\nu L_\nu$  to a power somewhat less than unity<sup>13</sup>. The truth is probably somewhere in between this result and that obtained for the blob energy  $E$ , i.e., very close to a linear dependence. Note that Russell et al. (2013) ignore altogether the fact that the jet blob transitions from optically thick to thin at light curve maximum, thereby missing a key piece of information. As a result, they do not have an analytic estimate of  $R$  and need to estimate  $t_{\text{jet}}$  from the poorly constrained rise time to maximum of the radio flux.

### 7.4.4 On Resolving the Controversy

In our view, the significant challenge posed by Russell et al. (2013) is whether GRO J1655–40 did or did not produce a strong radio flare during its 2005 outburst (Section 7.4.2); a similar challenge is posed for the 2002 outburst of 4U 1543–47 (Narayan & McClintock 2012). We maintain that both sources produced bright radio flares, but that they were missed because of the sparse radio coverage. On the other hand, Russell et al. (2013) and D. Russell (private communication) contend that the radio coverage was adequate to detect the strong flares during their decay phase, and they conclude that neither

<sup>12</sup> The ejection apparently shuts off, coincidentally, as the jet becomes optically thin.

<sup>13</sup> Using somewhat different assumptions, (Willott et al. 1999) estimated that kinetic jet kinetic luminosities of radio galaxies should vary as  $(\nu L_\nu)^{6/7}$ , i.e., a slope again close to but less than unity.



source produced a strong flare. This controversy cannot be firmly decided because the radio data collected for these events are inadequate.

Fortunately, we can expect the controversy to be settled relatively soon via radio observations of transient outburst events using new facilities such as the MeerKAT array (assuming a continuing capability to monitor the X-ray sky), and by the continual progress in obtaining secure measurements of the spins of transient black holes. MeerKAT, a forerunner of the SKA, is an array of 64 dishes scheduled for commissioning in 2014–2015 that will have outstanding sensitivity. R. Fender and P. Woudt, the PIs of the science project ThunderKAT, will obtain definitive measurements of all bright black-hole transients at high cadence (R. Fender, private communication).

## 8 Conclusions and Future Prospects

The continuum-fitting method has a number of virtues. A principal one is the simple and elegant model upon which it is based, namely the model of a thin, viscous accretion disk. This model was anticipated and developed well before the existence of black holes was established (e.g., Lynden-Bell 1969). Shortly thereafter, the analytic theory of thin disks was fully developed, an effort that culminated in the workhorse NT model (Novikov & Thorne 1973). The most important predictions of the model have been validated recently via GRMHD simulations (Sections 4.2 and 5.2). This venerable model, with the addition of a model of the disk’s atmosphere (Sections 3.1 and 5.3), measurements of three key parameters ( $D$ ,  $i$  and  $M$ ), and suitable X-ray data, allows one to estimate the inner-disk radius. Meanwhile, an abundance of strong observational and theoretical evidence allows one to identify the inner-disk radius with the radius of the ISCO, which is simply related to the spin of the black hole.

Another key virtue of the continuum-fitting method is an abundance of data for which the thermal disk component is strongly dominant. For most stellar black holes, one has many suitable archival spectra for which only a few percent or less of the thermal seed photons are upscattered by a hot corona into a Compton tail component of emission. In short: The continuum-fitting model is tried and true, and there is an abundance of suitable data for many stellar black holes obtained for the simplest and best understood state of an accreting black hole, namely, an optically-thick thermal disk.

The spins and masses of ten stellar black holes are given in Table 1. Their spins span the full range of prograde values, and their masses range from 6 – 16  $M_{\odot}$ . Setting aside the extreme spin of the transient GRS 1915+105, the three persistent black holes have higher spins and larger masses than their transient cousins. Furthermore, the high spins of these persistent, young black holes are unlikely to have been achieved via accretion torques, which implies that their spins are natal. The spins and masses of the ten black holes in Table 1 provide their complete description and are the essential data for testing astrophysical models of how an accreting black hole interacts with its environment. They are likewise essential data for underpinning the physical theory of black holes, and for ultimately attempting tests of the no-hair theorem by, e.g., observing deviations from the multipoles predicted by the Kerr metric, all of which are functions of just the two parameters  $a_*$  and  $M$  (Vigeland & Hughes 2010; Johannsen & Psaltis 2010, 2011; Bambi 2013).

To date, the most important application of the data in Table 1 is to one class of jets, namely, ballistic jets that are produced in major, Eddington-limited outbursts of black

holes in transient systems. For such outbursts the peak radio luminosities of five of these microquasars correlate strongly with their spins, increasing by a factor of  $\sim 1000$  as spin increases from  $\sim 0$  to  $> 0.95$ . Meanwhile, a simple synchrotron jet model shows radio luminosity to be a good proxy for jet power. As Narayan et al. (2013) discuss in detail, the fitted relationship between jet power and spin (Figure 6b) is not only a validation of the classic model of Blandford & Znajek (1977), it was also anticipated by GRMHD simulations showing that a jet can extract energy directly from a spinning black hole.

During the next several years, one can hope to double the number of black holes with spins measured via the continuum-fitting method. It will be equally important to improve the quality of each measurement, largely by obtaining more accurate measurements of the parameters  $D$ ,  $i$  and  $M$ , but also by making methodological advances and by pursuing more advanced GRMHD and atmosphere models of thin disks. The payoff for this effort will be the widening applications of these spin data to problems in astrophysics and physics.

Especially important will be the possibility of validating both the continuum-fitting and Fe-line methods by comparing spin results obtained for individual stellar black holes. The validation of the Fe-line method is particularly important because it is the most direct approach to measuring the spins of AGN. Presently, concordant results are being obtained using these two leading methods (e.g., Steiner et al. 2011, 2012b; Gou et al. 2011; Fabian et al. 2012; Reynolds 2013).

Two other methods for measuring the spins of stellar black holes appear promising, namely, via X-ray polarimetry (Dovčiak et al. 2008; Li et al. 2009; Schnittman & Krolik 2009) and high-frequency quasiperiodic oscillations (Török et al. 2005; Remillard & McClintock 2006; Belloni et al. 2012). The former method is stymied by a lack of data, and the latter by the lack of an adequate model. It is reasonable to hope that the mass and spin data in Table 1 will assist in identifying the appropriate physical model for the high-frequency QPOs. Because spin is such a critical parameter, it is important to attempt to measure it by as many methods as possible, as this will arguably provide our best check on the results. Stellar black holes are central to this effort because all of the methods of measuring spin mentioned above can be applied to them.

**Acknowledgements** The authors thank S. W. Davis for important input on Section 5.3. We also thank C. Brocksopp, E. Kuulkers, M. L. McCollough, C. Sánchez-Fernández and C. Zurita for help in preparing Figure 2; J. García and T. Fragos for their comments on a version of the manuscript; R. Fender for discussions on MeerKAT; and an anonymous referee for several important criticisms. JEM was supported in part by NASA grant NNX11AD08G and RN by NASA grant NNX11AE16G. JFS was supported by NASA Hubble Fellowship grant HST-HF-51315.01.

## References

- Abe, Y., Fukazawa, Y., Kubota, A., Kasama, D., & Makishima, K. 2005, PASJ, 57, 629  
 Abramowicz, M. A., & Fragile, P. C. 2013, Living Reviews in Relativity, 16, 1  
 Afshordi, N., & Paczyński, B. 2003, Astrophys. J., 592, 354  
 Arnaud, K. A. 1996, in Astronomical Society of the Pacific Conference Series, Vol. 101, Astronomical Data Analysis Software and Systems V, ed. G. H. Jacoby & J. Barnes, 17  
 Balbus, S. A., & Hawley, J. F. 1998, Reviews of Modern Physics, 70, 1  
 Bambi, C. 2013, The Astronomical Review, 8, 010000  
 Bardeen, J. M. 1970, Nature, 226, 64  
 Bardeen, J. M., & Petterson, J. A. 1975, Astrophys. J., 195, L65

- Bardeen, J. M., Press, W. H., & Teukolsky, S. A. 1972, *Astrophys. J.*, 178, 347
- Beckwith, K., Hawley, J. F., & Krolik, J. H. 2008, *Astrophys. J.*, 678, 1180
- Begelman, M. C., King, A. R., & Pringle, J. E. 2006, *MNRAS*, 370, 399
- Belloni, T. M., Sanna, A., & Méndez, M. 2012, *MNRAS*, 426, 1701
- Blandford, R. D., & Znajek, R. L. 1977, *MNRAS*, 179, 433
- Bolton, C. T. 1972, *Nature*, 235, 271
- Bradt, H. V. D., & McClintock, J. E. 1983, *ARA&A*, 21, 13
- Brocksopp, C., et al. 2002, *MNRAS*, 331, 765
- 2006, *MNRAS*, 365, 1203
- Campanelli, M., Lousto, C. O., & Zlochower, Y. 2006, *Phys. Rev. D*, 74, 041501
- Cantrell, A. G., et al. 2010, *Astrophys. J.*, 710, 1127
- Chandrasekhar, S. 1975, *Shakespeare, Newton and Beethoven: or Patterns of creativity* (Chicago: University of Chicago Press)
- Charles, P. A., & Coe, M. J. 2006, *Optical, ultraviolet and infrared observations of X-ray binaries*, ed. W. H. G. Lewin & M. van der Klis, 215–265
- Cooke, R., Bland-Hawthorn, J., Sharp, R., & Kuncic, Z. 2008, *Astrophys. J.*, 687, L29
- Cowley, A. P., Crampton, D., Hutchings, J. B., Remillard, R., & Penfold, J. E. 1983, *Astrophys. J.*, 272, 118
- Czerny, B., Hryniewicz, K., Nikolajuk, M., & Sądowski, A. 2011, *MNRAS*, 415, 2942
- Damour, T., Ruffini, R., Hanni, R. S., & Wilson, J. R. 1978, *Phys. Rev. D*, 17, 1518
- Davis, S. W., Blaes, O. M., Hirose, S., & Krolik, J. H. 2009, *Astrophys. J.*, 703, 569
- Davis, S. W., Blaes, O. M., Hubeny, I., & Turner, N. J. 2005, *Astrophys. J.*, 621, 372
- Davis, S. W., Done, C., & Blaes, O. M. 2006, *Astrophys. J.*, 647, 525
- Davis, S. W., & Hubeny, I. 2006, *ApJS*, 164, 530
- Dexter, J., & Fragile, P. C. 2011, *Astrophys. J.*, 730, 36
- Done, C., & Davis, S. W. 2008, *Astrophys. J.*, 683, 389
- Dovčiak, M., Muleri, F., Goosmann, R. W., Karas, V., & Matt, G. 2008, *MNRAS*, 391, 32
- Fabian, A. C., Rees, M. J., Stella, L., & White, N. E. 1989, *MNRAS*, 238, 729
- Fabian, A. C., et al. 2012, *MNRAS*, 424, 217
- Falcke, H., Körding, E., & Markoff, S. 2004, *Astron. Astrophys.*, 414, 895
- Farr, W. M., Sravan, N., Cantrell, A., Kreidberg, L., Bailyn, C. D., Mandel, I., & Kalogera, V. 2011, *Astrophys. J.*, 741, 103
- Fender, R. 2006, *Jets from X-ray binaries*, ed. W. H. G. Lewin & M. van der Klis, 381–419
- Fender, R., & Belloni, T. 2004, *ARA&A*, 42, 317
- Fender, R. P., Belloni, T. M., & Gallo, E. 2004, *MNRAS*, 355, 1105
- Fender, R. P., Gallo, E., & Russell, D. 2010, *MNRAS*, 406, 1425
- Fender, R. P., Garrington, S. T., McKay, D. J., Muxlow, T. W. B., Pooley, G. G., Spencer, R. E., Stirling, A. M., & Waltman, E. B. 1999, *MNRAS*, 304, 865
- Fender, R. P., Stirling, A. M., Spencer, R. E., Brown, I., Pooley, G. G., Muxlow, T. W. B., & Miller-Jones, J. C. A. 2006, *MNRAS*, 369, 603
- Fragos, T., et al. 2013, *Astrophys. J.*, 764, 41
- Fragos, T., Tremmel, M., Rantsiou, E., & Belczynski, K. 2010, *Astrophys. J.*, 719, L79
- Frank, J., King, A., & Raine, D. J. 2002, *Accretion Power in Astrophysics: Third Edition*
- Gallo, E., Fender, R. P., & Pooley, G. G. 2003, *MNRAS*, 344, 60
- Gammie, C. F. 1999, *Astrophys. J.*, 522, L57
- Ghez, A. M., et al. 2008, *Astrophys. J.*, 689, 1044
- Gierliński, M., & Done, C. 2004, *MNRAS*, 347, 885
- Gierliński, M., Maciołek-Niedźwiecki, A., & Ebisawa, K. 2001, *MNRAS*, 325, 1253
- Gillessen, S., Eisenhauer, F., Trippe, S., Alexander, T., Genzel, R., Martins, F., & Ott, T. 2009, *Astrophys. J.*, 692, 1075
- Gou, L., et al. 2009, *Astrophys. J.*, 701, 1076
- 2011, *Astrophys. J.*, 742, 85
- Gou, L., McClintock, J. E., Steiner, J. F., Narayan, R., Cantrell, A. G., Bailyn, C. D., & Orosz, J. A. 2010, *Astrophys. J.*, 718, L122
- Greene, J., Bailyn, C. D., & Orosz, J. A. 2001, *Astrophys. J.*, 554, 1290
- Gültekin, K., et al. 2009, *Astrophys. J.*, 695, 1577
- Heinz, S., & Sunyaev, R. A. 2003, *MNRAS*, 343, L59
- Herrnstein, J. R., Moran, J. M., Greenhill, L. J., & Trotter, A. S. 2005, *Astrophys. J.*, 629, 719
- Hirose, S., Krolik, J. H., & Blaes, O. 2009, *Astrophys. J.*, 691, 16

- Hjellming, R. M., & Johnston, K. J. 1988, *Astrophys. J.*, 328, 600
- Hubeny, I., & Lanz, T. 1995, *Astrophys. J.*, 439, 875
- Johannsen, T., & Psaltis, D. 2010, *Astrophys. J.*, 716, 187
- . 2011, *Phys. Rev. D*, 83, 124015
- Jolley, E. J. D., Kuncic, Z., Bicknell, G. V., & Wagner, S. 2009, *MNRAS*, 400, 1521
- Kato, S., Fukue, J., & Mineshige, S. 2008, *Black-Hole Accretion Disks — Towards a New Paradigm*
- Kelly, B. C. 2007, *Astrophys. J.*, 665, 1489
- King, A. R., & Kolb, U. 1999, *MNRAS*, 305, 654
- Koide, S., Shibata, K., Kudoh, T., & Meier, D. L. 2002, *Science*, 295, 1688
- Kolehmainen, M., & Done, C. 2010, *MNRAS*, 406, 2206
- Krolik, J. H. 1999, *Astrophys. J.*, 515, L73
- Kubota, A., & Makishima, K. 2004, *Astrophys. J.*, 601, 428
- Kubota, A., Makishima, K., & Ebisawa, K. 2001, *Astrophys. J.*, 560, L147
- Kulkarni, A. K., et al. 2011, *MNRAS*, 414, 1183
- Lee, C.-H., Brown, G. E., & Wijers, R. A. M. J. 2002, *Astrophys. J.*, 575, 996
- Li, L., Narayan, R., & McClintock, J. E. 2009, *Astrophys. J.*, 691, 847
- Li, L., Zimmerman, E. R., Narayan, R., & McClintock, J. E. 2005, *ApJS*, 157, 335
- Liu, J., McClintock, J. E., Narayan, R., Davis, S. W., & Orosz, J. A. 2008, *Astrophys. J.*, 679, L37
- Lynden-Bell, D. 1969, *Nature*, 223, 690
- MacFadyen, A. I., & Woosley, S. E. 1999, *Astrophys. J.*, 524, 262
- Makishima, K., Maejima, Y., Mitsuda, K., Bradt, H. V., Remillard, R. A., Tuohy, I. R., Hoshi, R., & Nakagawa, M. 1986, *Astrophys. J.*, 308, 635
- Markoff, S., Nowak, M. A., & Wilms, J. 2005, *Astrophys. J.*, 635, 1203
- McClintock, J. E., & Remillard, R. A. 1986, *Astrophys. J.*, 308, 110
- . 2006, *Black hole binaries*, ed. W. H. G. Lewin & M. van der Klis, 157–213
- McClintock, J. E., Remillard, R. A., Rupen, M. P., Torres, M. A. P., Steeghs, D., Levine, A. M., & Orosz, J. A. 2009, *Astrophys. J.*, 698, 1398
- McClintock, J. E., Shafee, R., Narayan, R., Remillard, R. A., Davis, S. W., & Li, L. 2006, *Astrophys. J.*, 652, 518
- McKinney, J. C. 2005, *Astrophys. J.*, 630, L5
- McKinney, J. C., & Blandford, R. D. 2009, *MNRAS*, 394, L126
- McKinney, J. C., & Gammie, C. F. 2004, *Astrophys. J.*, 611, 977
- Merloni, A., Heinz, S., & di Matteo, T. 2003, *MNRAS*, 345, 1057
- Middleton, M., Done, C., Gierliński, M., & Davis, S. W. 2006, *MNRAS*, 373, 1004
- Mirabel, I. F., & Rodríguez, I. 2003, *Science*, 300, 1119
- Mirabel, I. F., & Rodríguez, L. F. 1994, *Nature*, 371, 46
- . 1999, *ARA&A*, 37, 409
- Mitsuda, K., et al. 1984, *PASJ*, 36, 741
- Moreno Méndez, E., Brown, G. E., Lee, C., & Park, I. H. 2008, *Astrophys. J.*, 689, L9
- Narayan, R., & McClintock, J. E. 2005, *Astrophys. J.*, 623, 1017
- . 2008, *New A Rev.*, 51, 733
- . 2012, *MNRAS*, 419, L69
- Narayan, R., McClintock, J. E., & Tchekhovskoy, A. 2013, to appear in *Relativity and Gravitation: 100 Years after Einstein in Prague*, eds. J. Bicak, T. Ledvinka
- Noble, S. C., & Krolik, J. H. 2009, *Astrophys. J.*, 703, 964
- Noble, S. C., Krolik, J. H., & Hawley, J. F. 2010, *Astrophys. J.*, 711, 959
- Noble, S. C., Krolik, J. H., Schnittman, J. D., & Hawley, J. F. 2011, *Astrophys. J.*, 743, 115
- Novikov, I. D., & Thorne, K. S. 1973, in *Black Holes (Les Astres Occlus)*, ed. A. Giannaras, 343–450
- Nowak, M. A., Wilms, J., Pottschmidt, K., Schulz, N., Maitra, D., & Miller, J. 2012, *Astrophys. J.*, 744, 107
- Orosz, J. A. 2003, in *IAU Symposium, Vol. 212, A Massive Star Odyssey: From Main Sequence to Supernova*, ed. K. van der Hucht, A. Herrero, & C. Esteban, 365
- Orosz, J. A., McClintock, J. E., Aufdenberg, J. P., Remillard, R. A., Reid, M. J., Narayan, R., & Gou, L. 2011a, *Astrophys. J.*, 742, 84
- Orosz, J. A., et al. 2007, *Nature*, 449, 872
- . 2009, *Astrophys. J.*, 697, 573

- Orosz, J. A., Steiner, J. F., McClintock, J. E., Torres, M. A. P., Remillard, R. A., Bailyn, C. D., & Miller, J. M. 2011b, *Astrophys. J.*, 730, 75
- Özel, F., Psaltis, D., Narayan, R., & McClintock, J. E. 2010, *Astrophys. J.*, 725, 1918
- Paczynski, B. 2000, arXiv:astro-ph/0004129v1
- Page, D. N., & Thorne, K. S. 1974, *Astrophys. J.*, 191, 499
- Penna, R. F., McKinney, J. C., Narayan, R., Tchekhovskoy, A., Shafee, R., & McClintock, J. E. 2010, *MNRAS*, 408, 752
- Penna, R. F., Sądowski, A., & McKinney, J. C. 2012, *MNRAS*, 420, 684
- Penrose, R. 1969, *Nuovo Cimento Rivista Serie*, 1, 252
- Reid, M. J., McClintock, J. E., Narayan, R., Gou, L., Remillard, R. A., & Orosz, J. A. 2011, *Astrophys. J.*, 742, 83
- Remillard, R. A., & McClintock, J. E. 2006, *ARA&A*, 44, 49
- Remillard, R. A., McClintock, J. E., & Bailyn, C. D. 1992, *Astrophys. J.*, 399, L145
- Reynolds, C. S. 2013, arXiv:1302.3260 [astro-ph.HE]
- Riffert, H., & Herold, H. 1995, *Astrophys. J.*, 450, 508
- Ross, R. R., & Fabian, A. C. 2007, *MNRAS*, 381, 1697
- Ruffini, R., & Wilson, J. R. 1975, *Phys. Rev. D*, 12, 2959
- Rupen, M. P., Mioduszewski, A. J., & Dhawan, V. 2005, *ATel #434*
- Russell, D. M., Gallo, E., & Fender, R. P. 2013, *MNRAS*, 431, 405
- Sánchez-Fernández, C., Castro-Tirado, A. J., Giménez, A., Zurita, C., Casares, J., & Lund, N. 2001, *Astrophysics and Space Science Supplement*, 276, 51
- Schnittman, J. D., & Krolik, J. H. 2009, *Astrophys. J.*, 701, 1175
- Shafee, R., McClintock, J. E., Narayan, R., Davis, S. W., Li, L., & Remillard, R. A. 2006, *Astrophys. J.*, 636, L113
- Shafee, R., McKinney, J. C., Narayan, R., Tchekhovskoy, A., Gammie, C. F., & McClintock, J. E. 2008a, *Astrophys. J.*, 687, L25
- Shafee, R., Narayan, R., & McClintock, J. E. 2008b, *Astrophys. J.*, 676, 549
- Shahbaz, T., Ringwald, F. A., Bunn, J. C., Naylor, T., Charles, P. A., & Casares, J. 1994, *MNRAS*, 271, L10
- Shakura, N. I., & Sunyaev, R. A. 1973, *Astron. Astrophys.*, 24, 337
- Smale, A. P., & Boyd, P. T. 2012, *Astrophys. J.*, 756, 146
- Steeeghs, D., McClintock, J. E., Parsons, S. G., Reid, M. J., Littlefair, S., & Dhillion, V. S. 2013, *Astrophys. J.*, 768, 185
- Steiner, J. F., & McClintock, J. E. 2012, *Astrophys. J.*, 745, 136
- Steiner, J. F., McClintock, J. E., & Narayan, R. 2013, *Astrophys. J.*, 762, 104
- Steiner, J. F., McClintock, J. E., & Reid, M. J. 2012a, *Astrophys. J.*, 745, L7
- Steiner, J. F., McClintock, J. E., Remillard, R. A., Gou, L., Yamada, S., & Narayan, R. 2010, *Astrophys. J.*, 718, L117
- Steiner, J. F., McClintock, J. E., Remillard, R. A., Narayan, R., & Gou, L. 2009a, *Astrophys. J.*, 701, L83
- Steiner, J. F., Narayan, R., McClintock, J. E., & Ebisawa, K. 2009b, *PASP*, 121, 1279
- Steiner, J. F., et al. 2012b, *MNRAS*, 427, 2552
- . 2011, *MNRAS*, 416, 941
- Straub, O., et al. 2011, *Astron. Astrophys.*, 533, A67
- Tanaka, Y., & Lewin, W. H. G. 1995, in *X-ray Binaries*, ed. W. H. G. Lewin, J. van Paradijs, & E. P. J. van den Heuvel, 126–174
- Tanaka, Y., et al. 1995, *Nature*, 375, 659
- Tchekhovskoy, A., Narayan, R., & McKinney, J. C. 2010, *Astrophys. J.*, 711, 50
- . 2011, *MNRAS*, 418, L79
- Török, G., Abramowicz, M. A., Kluźniak, W., & Stuchlík, Z. 2005, *Astron. Astrophys.*, 436, 1
- van der Laan, H. 1966, *Nature*, 211, 1131
- Vigeland, S. J., & Hughes, S. A. 2010, *Phys. Rev. D*, 81, 024030
- Wang, X. Y., Dai, Z. G., & Lu, T. 2003, *Astrophys. J.*, 592, 347
- Webster, B. L., & Murdin, P. 1972, *Nature*, 235, 37
- White, N. E., & Ghosh, P. 1998, *Astrophys. J.*, 504, L31
- White, N. E., Nagase, F., & Parmar, A. N. 1995, *X-ray Binaries*, ed. W. H. G. Lewin, J. van Paradijs & E. P. J. van den Heuvel, 1
- Willott, C. J., Rawlings, S., Blundell, K. M., & Lacy, M. 1999, *MNRAS*, 309, 1017
- Wilms, J., Allen, A., & McCray, R. 2000, *Astrophys. J.*, 542, 914
- Wong, T.-W., Valsecchi, F., Fragos, T., & Kalogera, V. 2012, *Astrophys. J.*, 747, 111

- Woosley, S. E. 1993, *Astrophys. J.*, 405, 273
- Woosley, S. E., & Heger, A. 2006, *Astrophys. J.*, 637, 914
- Zdziarski, A. A., Mikołajewska, J., & Belczyński, K. 2013, *MNRAS*, 429, L104
- Zhang, S. N., Cui, W., & Chen, W. 1997, *Astrophys. J.*, 482, L155
- Zhu, Y., Davis, S. W., Narayan, R., Kulkarni, A. K., Penna, R. F., & McClintock, J. E. 2012, *MNRAS*, 424, 2504
- Zimmerman, E. R., Narayan, R., McClintock, J. E., & Miller, J. M. 2005, *Astrophys. J.*, 618, 832

